
[All ETDs from UAB](#)

[UAB Theses & Dissertations](#)

2018

A Computational Approach To Analyze Vortex Induced Vibration For A Flexible Riser

Ibrahim Bilgin
University of Alabama at Birmingham

Follow this and additional works at: <https://digitalcommons.library.uab.edu/etd-collection>



Part of the [Engineering Commons](#)

Recommended Citation

Bilgin, Ibrahim, "A Computational Approach To Analyze Vortex Induced Vibration For A Flexible Riser" (2018). *All ETDs from UAB*. 1168.

<https://digitalcommons.library.uab.edu/etd-collection/1168>

This content has been accepted for inclusion by an authorized administrator of the UAB Digital Commons, and is provided as a free open access item. All inquiries regarding this item or the UAB Digital Commons should be directed to the [UAB Libraries Office of Scholarly Communication](#).

A COMPUTATIONAL APPROACH TO ANALYZE VORTEX INDUCED
VIBRATION FOR A FLEXIBLE RISER

by

IBRAHIM BILGIN

ROY KOOMULLIL, CHAIR
LEE MORADI
HESSAM TAHERIAN

A THESIS

Submitted to the graduate faculty of The University of Alabama at Birmingham,
in partial fulfillment of the requirements for the degree of
Master of Science

BIRMINGHAM, ALABAMA

2018

Copyright by
Ibrahim Bilgin
2018

A COMPUTATIONAL APPROACH TO ANALYZE VORTEX INDUCED VIBRATION FOR A FLEXIBLE RISER

IBRAHIM BILGIN

MECHANICAL ENGINEERING

ABSTRACT

Vortex shedding is an oscillating flow behind blunt bodies when fluid flows past it. One of the consequences of vortex shedding is the vortex-induced vibrations (VIV), which happens in numerous engineering structures such as bridge, heat exchangers, marine cables, electrical power lines, and risers in petroleum production. A critical application of VIV is the risers used in petroleum industries, which connects between sea surface and sea base. A failure of risers and platforms can result in enormous economic and catastrophic environmental problems. Therefore, understanding VIV is essential to estimate fatigue damage of the offshore systems.

This thesis describes a computational approach to analyze VIV of a flexible riser in a uniform current using a fluid-structure interaction (FSI) approach. Different components of the ANSYS/Fluent software suite are used to analyze this problem. This computational approach is validated using the experimental data on a flexible riser tested at the MARINTEK by ExxonMobil Upstream Research Company (URC). The computed root mean square (RMS) values of the amplitude of vibrations in the in-line (IL) and cross-flow (CF) directions are compared with the experimental data, and they are found to be in good agreement with each other. This validated model could be used for the estimation of the effectiveness of VIV suppression systems for flexible risers.

Keywords: Fluid-structure interaction (FSI), Vortex-induced vibration (VIV),
Suppression, Riser, Computational fluid dynamics (CFD)

DEDICATION

The thesis is dedicated to my wife Merve Morkoc Bilgin who has supported me her encouragement and understanding since the beginning of this research work.

Also, this is dedicated to my son Bera Bilgin who has been an excellent source of motivation.

ACKNOWLEDGMENTS

I would like to thank my advisor, Dr. Roy Koomullil, for his helpful guidance and support during this research. He has a unique mentor throughout my studying in the University of Alabama at Birmingham (UAB).

Thanks also go to my sponsor, Turkish Petroleum Corporation (TPAO) to support my higher education and to pursue my dreams.

Finally, thanks to my mother and father for their encouragement and my wife for her patience, inspiring and love.

TABLE OF CONTENTS

	<i>Page</i>
ABSTRACT	iii
DEDICATION	v
ACKNOWLEDGMENTS	vi
LIST OF TABLES.....	ix
LIST OF FIGURES	x
ABBREVIATIONS	xiii
CHAPTER 1 INTRODUCTION	1
1.1 Problem Statement.....	6
1.2 Objectives	8
CHAPTER 2 LITERATURE REVIEW	9
2.1 Experimental Approach	9
2.1.1 <i>MARINTEK Experimental Data</i>	9
2.1.1.1 <i>Parameters of Experimental Data</i>	10
2.1.1.2 <i>Definition of Test Rig</i>	11
2.1.1.3 <i>Instrumentation and Measurements</i>	12
2.1.2 <i>Deepstar Company</i>	14
2.1.2.1 <i>The parameter of Experimental Data</i>	14
2.1.2.2 <i>Definition of Test Rig</i>	16
2.1.2.3 <i>Measurement</i>	17
2.2 Numerical Approach.....	19
CHAPTER 3 METHODOLOGY.....	22
3.1 Fluid Solver.....	24
3.2 Structural Solver	25
3.3 Modal Analysis	25
3.4 FSI Analysis using ANSYS	26

CHAPTER 4	RESULTS AND DISCUSSIONS	28
4.1	Modal Analysis	29
4.2	Fluid Flow Analysis	32
4.3	Estimation of Speed-up and the Number of Processors.....	48
4.4	Convergence of the Fluid and FSI Analyses.....	50
4.5	Results from FSI Analysis and Comparison with the Experimental Data..	51
4.6	The Riser Dynamic Response.....	57
4.7	Comparison of RMS values of the Amplitudes of Oscillation with Experimental Data for a Freestream Velocity of 0.42 m/s	58
CHAPTER 5	SUMMARY	61
CHAPTER 6	FUTURE WORK	63
6.1	The Geometry of the Riser with Fairings	63
6.2	The Geometry of the Riser with the Strakes.....	64
6.3	Modal Analysis for Riser with Suppression	64
6.4	Fluid Analysis of the Riser with the Fairing.....	66
REFERENCES	72

LIST OF TABLES

<i>Table</i>	<i>Page</i>
1. Riser model parameters.....	10
2. Strake properties	11
3. Location of transducers (Lehn, 2003).....	14
4. Pipe properties	15
5. Properties of the riser covered strakes	16
6. Properties of the riser covered fairing.....	16
7. The properties of the riser model used.....	29
8. Eigen frequencies for the flexible riser.....	32
9. Frequency and Strouhal number from fluid flow analysis.....	46
10. Eigenfrequencies for the flexible riser with the fairing	65
11. Eigenfrequencies for the flexible riser with the strakes.....	66
12. Frequency and Strouhal number from fluid flow analysis.....	70

LIST OF FIGURES

<i>Figure</i>	<i>Page</i>
1.1. Von Karman vortex (Kármán, 1994).....	1
1.2. Regimes of the fluid flow past a circular cylinder (Blevins, 1990).....	3
1.3. Sketch of a riser system	4
1.4. Suppression devices (Zdravkovich, 1981).....	6
2.1. Sketch of the test rig (Lehn, 2003).....	12
2.2. Sketch of the strain sensor locations (Gao et al., 2016).....	13
2.3. Set-up for the Gulf Stream Experiments 2006; (Jaiswal & Vandiver, 2007)	17
2.4. Cross-Section of the pipe from Gulf Stream test: (Jaiswal & Vandiver, 2007)	18
2.5. The arrangement of strain gauges in a quadrant for Gulf Stream test; (Jaiswal & Vandiver, 2007)	19
3.1. Schematic diagram of a loosely-coupled FSI approach.....	23
3.2. Schematic of system coupling setup in ANSYS.....	27
4.1. The geometry of the riser.....	30
4.2. The mesh on the riser.....	30
4.3. Computational domain for fluid flow analysis	33
4.4. Block structure on top XY-plane	34
4.5. The number of divisions on the selected boundary segments.....	34
4.6. Mesh on top XY-plane.....	35
4.7. Mesh around the riser.....	35
4.8. Overall view of the coarse mesh.....	36

4.9. Overall view of the fine mesh.....	36
4.10. Drag history for the flow with a freestream velocity of 0.2 m/s.....	38
4.11. Power spectral density from drag history for the flow with a freestream; velocity of 0.2 m/s.....	39
4.12. Lift history for the flow with a freestream velocity of 0.2 m/s.....	40
4.13. Power spectral density from lift history for the flow with a freestream; velocity of 0.2 m/s.....	41
4.14. Drag history for the flow with a freestream velocity of 0.42 m/s.....	42
4.15. Power spectral density from drag history for the flow with a freestream; velocity of 0.42 m/s.....	43
4.16. Lift history for the flow with a freestream velocity of 0.42 m/s.....	44
4.17. Power spectral density from lift history for the flow with a freestream; velocity of 0.42 m/s.....	45
4.18. Vortex shedding at $z/L = 0.22$ of the riser at freestream; velocity, 0.2 m/s, on the coarse mesh	47
4.19. Vortex shedding at $z/L = 0.22$ of the riser at freestream; velocity, 0.2 m/s, on the fine mesh	47
4.20. Vortex shedding at $z/L = 0.22$ of the riser at freestream; velocity, 0.42 m/s, on the coarse mesh	48
4.21. Vortex shedding at $z/L = 0.22$ of the riser at freestream; velocity, 0.42 m/s, on the fine mesh	48
4.22. Speed-up obtained when using a different number of processors; for the fluid solver.....	49
4.23. Speed-up obtained when using a different number of processors; for the structural solver	50
4.24. The residual of the fluid analysis	51
4.25. The residual of the FSI analysis.....	51
4.26. Schematic diagram of the system coupling in ANSYS	52
4.27. Comparison of the RMS amplitudes in IL direction between fine and coarse; mesh systems with published data at freestream velocity = 0.2 m/s	54

4.28. Comparison of the RMS amplitudes in CF direction between fine and coarse; mesh systems with published data at freestream velocity = 0.2 m/s	54
4.29. Comparison of data from difference oscillation cycles in in-line (IL); direction on the coarse mesh.....	55
4.30. Comparison of data from difference oscillation cycles in cross-flow (CF); direction on the coarse mesh.....	55
4.31. Comparison of data from difference oscillation cycles in in-line (IL); direction on the fine mesh.....	56
4.32. Comparison of data from difference oscillation cycles in cross-flow (CF); direction on the fine mesh.....	56
4.33. Comparison of the envelopes in IL direction at a velocity of 0.2 m/s	57
4.34. Comparison of the envelopes in CF direction at a velocity of 0.2 m/s	58
4.35. Comparison of the RMS amplitudes in IL direction on the fine mesh; with published data at velocity = 0.42 m/s	59
4.36. Comparison of the RMS amplitudes in CF direction on the fine mesh; with published data at velocity = 0.42 m/s	60
6.1. The top view of the riser with the fairing	63
6.2. The top view of the riser with the strakes	64
6.3. Block structure on top XY-plane	67
6.4. The number of divisions on the selected boundary segments.....	67
6.5. Mesh on top XY-plane.....	68
6.6. Mesh around the fairing	68
6.7. Overall view of the coarse mesh	69
6.8. Power spectral density from lift history for the flow with a freestream; velocity of 0.2 m/s.....	70
6.9. Vortex shedding at $z/L = 0, 0.25, 0.5, 0.75, 1$ of the riser with the fairing; at freestream velocity, 0.2 m/s	71

ABBREVIATIONS

CFD	Computational Fluid Dynamics
FSI	Fluid-structure Interaction
VIV	Vortex-Induced Vibration
SST	Shear Stress Transport
RMS	Root Mean Square

CHAPTER 1 INTRODUCTION

Vortex shedding is an oscillating flow behind blunt bodies when fluid flows past it. This is characterized by periodic detachment of recirculating fluid from behind blunt bodies, and this separate fluid is carried downstream by the fluid flow. This phenomenon happens in many natural scenarios. One of the famous vortex shedding problems is the one from a circular cylinder, shown in Figure 1.1 (Kármán, 1994), and is named von Karman Vortex (Kármán, 1994). The frequency of vortex shedding is usually represented using a non-dimensional number called Strouhal number, which is defined as $St = \frac{fD}{U}$, where f is the frequency of vortex shedding, D is the characteristic length of the problem, and U is the freestream velocity.



Figure 1.1. Von Karman vortex (Kármán, 1994)

Vortex shedding is a strong function of the Reynolds number (Re), which is the ratio of inertial force to viscous force. For a circular cylinder, the Reynolds number is defined as $Re = \frac{U_\infty D}{\nu}$, where U_∞ is the stream velocity, D is the diameter of the cylinder, and ν is

the kinematic viscosity of the fluid. The dependency of vortex shedding from a cylinder and the resulting flow patterns on the Reynolds number are shown in Figure 1.2 (Blevins, 1990). At Reynolds number below five, the flow is fully attached without any separation. Reynolds number between 5 and 45, the flow separates from the cylinder and a symmetric pair of recirculation regions are formed behind the cylinder. In the Reynolds number range between 40 and 150, the recirculation regions detach from the body and periodic vortices are formed. In this range, the flow remains smooth and laminar. Transition to turbulent flow starts at Reynolds number 150, and the flow become fully turbulent when the Reynolds number reaches 3×10^5 . Periodic shedding of vortices is maintained in this Re range too. However, for the Reynolds number range $3 \times 10^5 < Re < 3.5 \times 10^6$, the flow become chaotic and disorganized, and the periodic vortices disappears. For Reynolds number above 3.5×10^6 , a regular vortex shedding is re-established with fully turbulent flow.

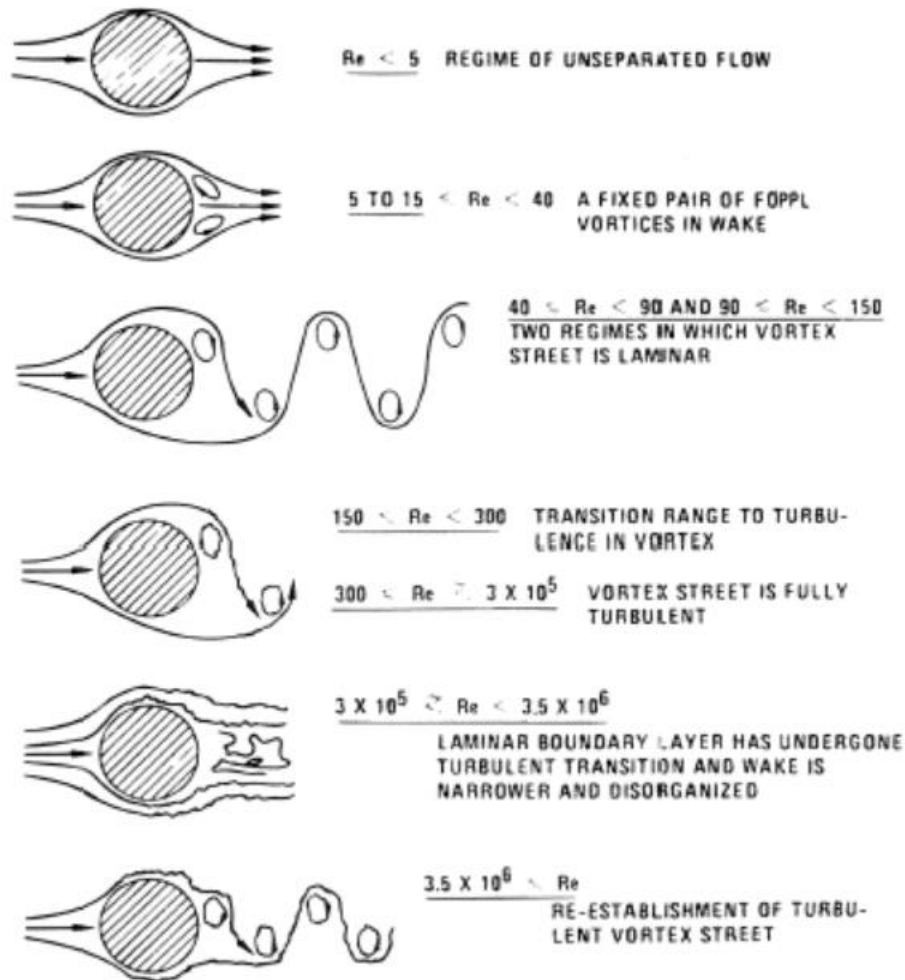


Figure 1.2. Regimes of the fluid flow past a circular cylinder (Blevins, 1990)

One of the consequences of vortex shedding is the vortex-induced vibrations (VIV), which happens in numerous engineering structures such as bridge, heat exchangers, marine cables, electrical power lines, and risers in petroleum production (Sarpkaya, 2004). Fluid flow around these structures causes periodic vortex shedding, and this in-turn causes periodic forces on the structures. The structures respond to these periodic forces by deformation, and the deformation causes changes in the forces exerted by the fluid. Catastrophic failure of the structure can occur when the frequency of the vortex shedding matches the natural frequency of the structure. In addition, VIV can create noise as well

as fatigue failures. Therefore, efficient control of VIV is significant in many engineering implementations. One of the most critical applications of VIV is the risers used in petroleum industries, which connects between sea surface and sea base as shown in Figure 1.3. Especially in this subsea industry, the failure of risers and platforms can result in enormous economic and catastrophic environmental problems.

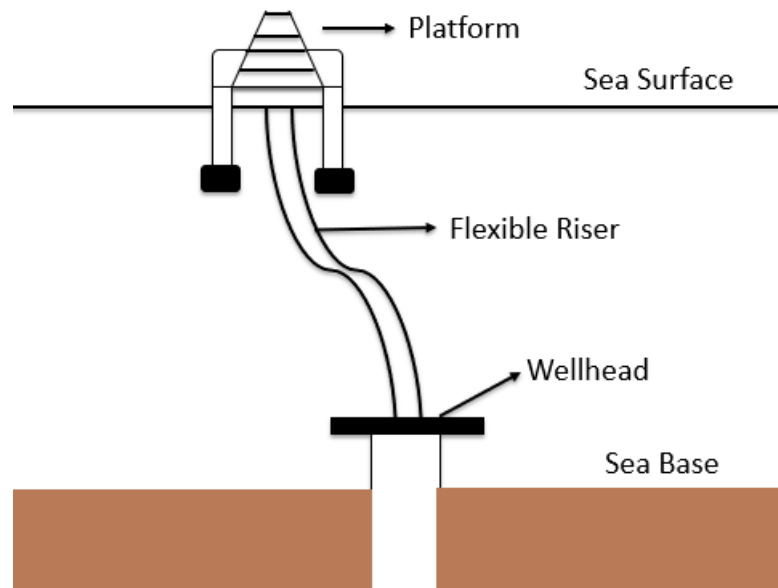


Figure 1.3. Sketch of a riser system

Progress has been made over the years on the analysis and mitigation of vortex-induced vibration problems. In the past few decades, the focus of many researchers was on VIV suppression. These methods for suppressing VIV can be categorized into active and passive controls (Choi, Jeon, & Kim, 2008). The active flow control techniques utilize smart sensors and actuators to make appropriate changes to the forces and the moments acting on the structures based on the external flow conditions. There are two methods in active controls, and they are called predetermined and interactive. A predetermined active control method involves the introduction of energy inputs without consideration for the

state of the flow field such as jet vectoring using piezoelectric actuators. The interactive method consists of feedforward and feedback control methods. While feedforward control methods involve sensors in the upstream of the actuator to measure the controlled flow field, feedback control methods involve sensors in the downstream of the actuator (Jahanmiri, 2010; Kral, 2000). Even though active controls can be more precise, it requires external power sources to operate. Passive flow control techniques utilize geometry modification to reduce the strength of the vortex shedding and the resulting vibrations. For these reasons, in offshore engineering applications, passive controls are mainly used (Bearman & Owen, 1998). The geometric modifications that are used in passive controls are shown in Figure 1.4 (Zdravkovich, 1981). Out of these, the most commonly used ones for risers are the helical strakes and the fairings.

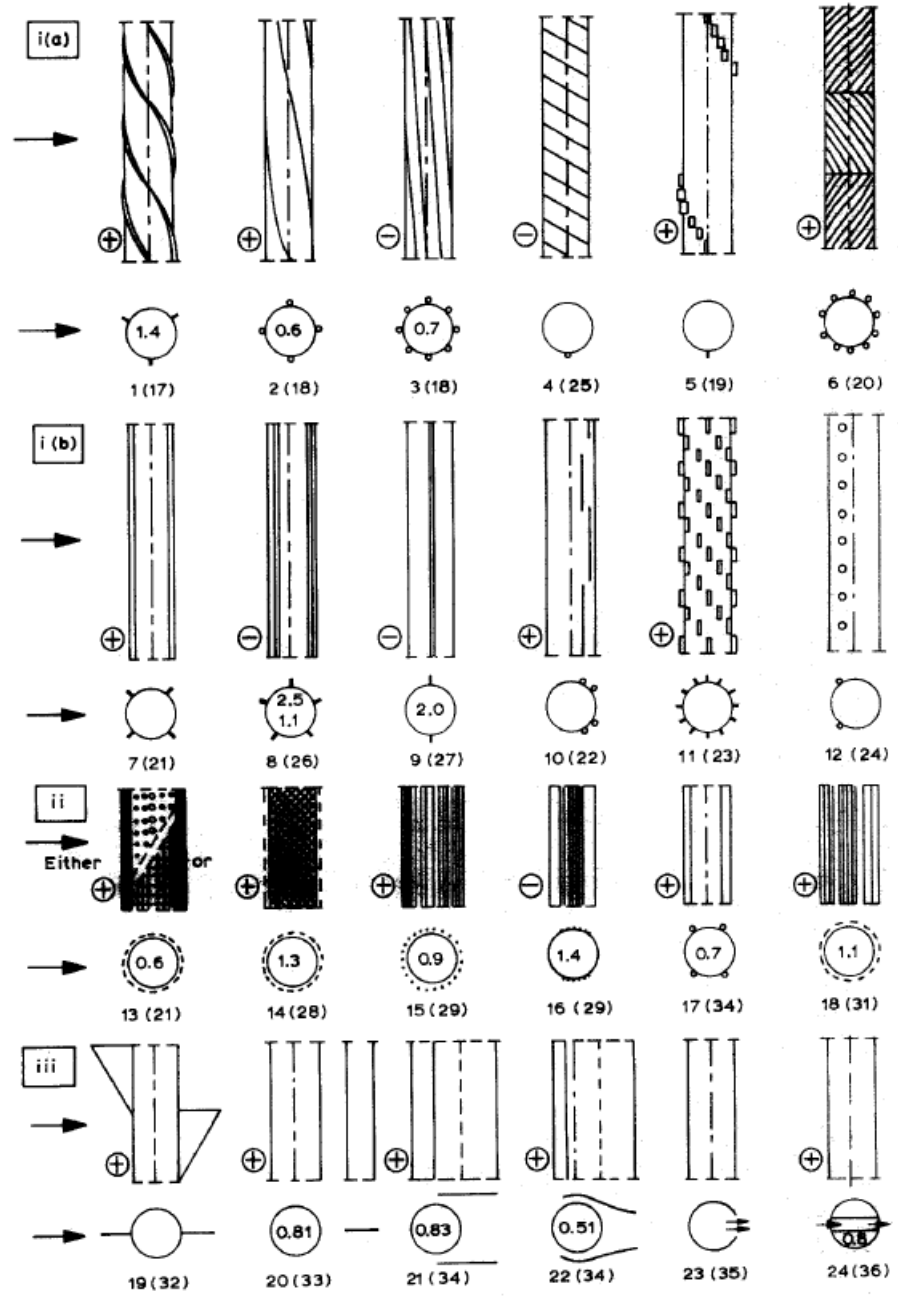


Figure 1.4. Suppression devices (Zdravkovich, 1981)

1.1 Problem Statement

It is crucial to estimate its fatigue life when it is installed. Failures will cost lots of environmental and economic impacts (Mukundan, Modarres-Sadeghi, Dahl, Hover, & Triantafyllou, 2009). This problem should be addressed before the installation of the risers.

Vortex-induced vibration (VIV) is an essential factor for fatigue damage in offshore systems and production risers. It is essential to understand the amplitude of vibration to predict the fatigue damage rate (Liao, 2001). Therefore, it is essential to study fittings on risers to reduce VIV. There are many challenges to address this issue, and a few of these are listed below:

- 1) Multi-disciplinary problem. For an accurate simulation of this problem, the governing equations for fluid and structures need to be solved in a coupled fashion. Also, the accuracy of one field simulation will affect the accuracy of the other. For example, prediction of a wrong excitation mode of vibration of the structures will affect the fluid forces. Similarly, the prediction of a wrong vortex shedding frequency will influence the excitation mode of the vibration of the structure.
- 2) Variability of the flow fields. The riser systems can face flows with different velocities and patterns. These include steady flows, unsteady flows, sheared flows, free surface, and wave patterns.
- 3) Large computational resource requirements. Fluid-structure interaction simulations are inherently CPU intensive. These will be critical especially during the initial design stages, where a wide range of designs needs to be evaluated. In addition, a well-validated FSI framework is required to accurately simulation VIV.
- 4) Design and manufacturing cost. To evaluate the effects of passive control systems, a parametric study needs to be carried to find the optimum configuration. In addition, production cost and manufacturability of the fittings need to be considered during the design process.

1.2 Objectives

The goal of this study is to develop a numerical approach to analyze VIV for risers in uniform currents using a computational fluid-structure interaction (FSI) approach. This study will offer insights into VIV response and displacement of flexible risers. The developed numerical approach could use to estimate the effectiveness of the passive controls.

CHAPTER 2 LITERATURE REVIEW

Suppression of vortex-induced vibration of a vertical riser has been investigated over the past decades. However, with the recent increase in offshore oil production, enhancement of VIV suppressors has regained attention by researchers. Installing a riser with suppressors could be efficient for low mass-damping systems under heavy environmental conditions especially offshore systems.

Comprehensive reviews of solutions from the simple and cheap suppressors such as helical strakes and fairings to expensive active control devices are available in the literature (Every, King, & Weaver, 1982; Zdravkovich, 1981). The literature on the analysis and suppression of VIV can be categorized into two groups: experimental and numerical approaches. A summary of the available literature on experimental testing and numerical simulations are summarized below.

2.1 Experimental Approach

2.1.1 *MARINTEK Experimental Data*

In Marintek's Ocean Basin laboratory, a high length-to-diameter ratio (L/D) flexible riser with or without suppression devices, strakes, and fairings, was tested under uniform and linearly varying shared currents (Lehn, 2003). In this experiment, measurements were made to acquire bending moments and accelerations in cross-flow (CF) direction and in in-line flow (IL) direction to investigate VIV under different types of currents. Furthermore, from the experimental measurements, a comparison of the multi-mode VIV response of risers was also made.

2.1.1.1 Parameters of Experimental Data

The parameters for the riser model used in the experiment are listed in Table 1 (Lehn, 2003). According to designing a riser, the vibration mode is an essential parameter to fatigue damage in this experimental data to create a riser to consider 8th vibration mode. The mass ratio of the bare riser, which is described as the total mass in air divided by the displaced mass, is also reported in the literature. The error band for the mass was reported as $\pm 2\%$.

Parameters	Values	SI units
Length	9.63	m
Outer Diameter	20	mm
Wall thickness	0.45	mm
Modulus of elasticity	1.025×10^{11}	N/m ²
Total mass in air	6.731	kg
Mass ratio	2.23	-

Table 1. Riser model parameters

In this set of experiments, the triple helix was made of silicone material and was bonded to the riser model with a specific pitch of 320 mm. The shape of strakes was triangular with a height of 5 mm and a width of 5 mm. The properties of the strakes are shown in Table 2 (Lehn, 2003).

Parameters	Values	SI units
Height	0.005	m
Width	0.005	m
Unit weight in air	0.245	N/m
Pitch/Outer Diameter	16	-

Table 2. Strake properties

2.1.1.2 Definition of Test Rig

The tests were carried out in a rotating test rig attached to a 10 m deep towing tank, as sketched in Figure 2.1 (Lehn, 2003). In this figure, A is a 13m long vertical cylinder with a diameter 0.485 m, B are two horizontal arms and opposite directions at the top of the cylinder, C is the horizontal arm at the bottom, and D is a sloping beam connected to the cylinder. The distance between D and the water surface is 0.15 m. The jointed arm E is attached to this beam, and it can be placed in different positions. Lastly, there is a spring system holds the arm, which behaves as a low heave damping with constant tension during the test. Also, it includes six springs, with a total vertical stiffness of 1593 N/m. The minimum and the maximum current speed of all models were 0.2 m/s and 2.3 m/s, respectively (Lehn, 2003).

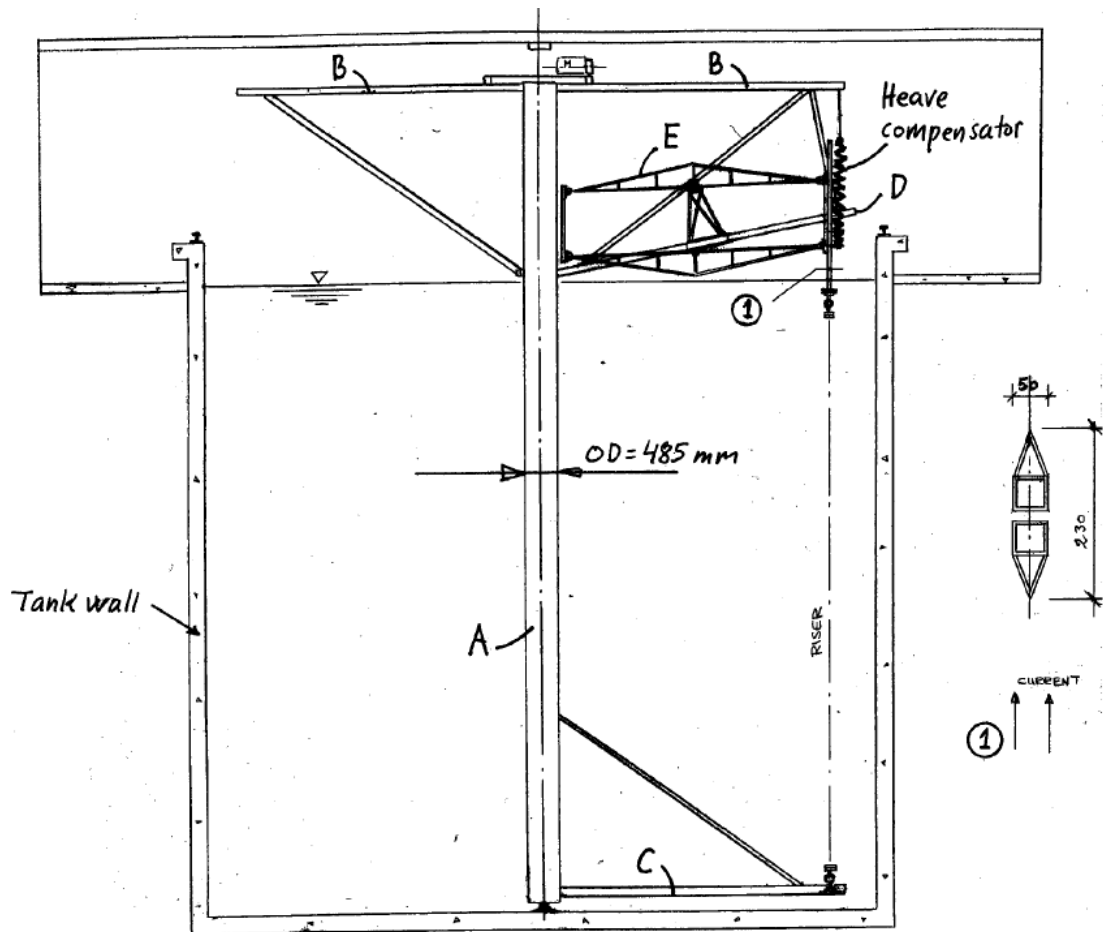


Figure 2.1. Sketch of the test rig (Lehn, 2003)

2.1.1.3 Instrumentation and Measurements

There were 68 transducers in the riser model. Out of these, 52 transducers were to measure the bending moments, with 35 in in-line (IL) direction and 17 in cross-flow (CF) direction. Figure 2.2 (Gao, Yang, Xiong, Wang, & Peng, 2016) illustrates the position of the strain gauges and accelerometers on the riser model.

Signal	Direction	Transducer
Accelerations of test rig upper end	x, y, and z	Linear accelerations
Accelerations of test rig lower end	x, y, and z	Linear accelerations
Riser force upper end	x, y, and z	Strain gauge transducer
Riser force lower end	x, y, and z	Strain gauge transducer
Riser top set-down	z	Linear spring-transducer system
The rotational speed test rig	Angular	Potentiometer

Table 3. Location of transducers (Lehn, 2003)

2.1.2 Deepstar Company

The Gulf Stream experiment was conducted offshore Miami in October 2006. This experiment was designed and performed by a team from the Massachusetts Institute of Technology (MIT) and was sponsored by Deepstar Company. This experiment was designed to better understand the behavior of structures with partially overlapped strakes. One of the main objectives was to acquire data to calibrate a VIV prediction software (Jaiswal & Vandiver, 2007).

2.1.2.1 The parameter of Experimental Data

The parameters of the riser model used in this experiment are listed in Table 4. The material of the pipe is a glass fiber epoxy composite. A mode of vibration, related to a modal frequency and a mode shape, is the number of half waves in the vibration

(Blevins & Plunkett, 1980). According to high mode numbers, the length and diameter of the pipe, 152.52 m and 3.6322 cm in outer diameter, respectively, were chosen. The density of the pipe is 1383.84 kg/g³ (Jaiswal & Vandiver, 2007).

Parameter	Value	Units
Inner Diameter	2.4892	cm
Outer Diameter	3.6322	cm
Modulus of Elasticity (E)	1.33 x 10 ⁶	N/m ²
Weight in air	7.6045	g/cm
Weight in water	1.9718	g/cm
Density	1383.84	g/cm ³
Length	152.52	m

Table 4. Pipe properties

In addition to a bare pipe, this experiment included pipes with both strake and fairing coverage. The strakes were a triple helix design and made of polyethylene, with a pitch to diameter 17.5. The height of the strake was 25% of the outer shell diameter. All other properties associated with the strakes are illustrated in Table 5. Also, the properties associated with the fairings are listed in Table 6.

Parameter	Value	Units
Length	14.0805	cm
Shell outer diameter	3.7846	cm
Shell inner diameter	3.3528	cm
Strake height	0.9525	cm
Wall thickness	0.2286	cm
Pitch/D	17.5	-
Weight / Length in air	1.636976 ± 10%	g/cm

Table 5. Properties of the riser covered strakes

Parameter	Value	Units
Length	37.9984	cm
Shell thickness	0.33528	cm
Shell inner diameter	3.5052	cm
Weight / Length in air	278.051896	g

Table 6. Properties of the riser covered fairing

2.1.2.2 *Definition of Test Rig*

The spooler was in the back of the ship. It loaded the pipe. The pipe was released into the water from the spooler. Although the weight in a railroad wheel in water is 725 lbs., the weight in a railroad wheel in the air is 805 lbs. The pipe was attached to the bottom of the pipe to provide tension. A schematic diagram of the experimental setup is shown in Figure 2.3 (Jaiswal & Vandiver, 2007).

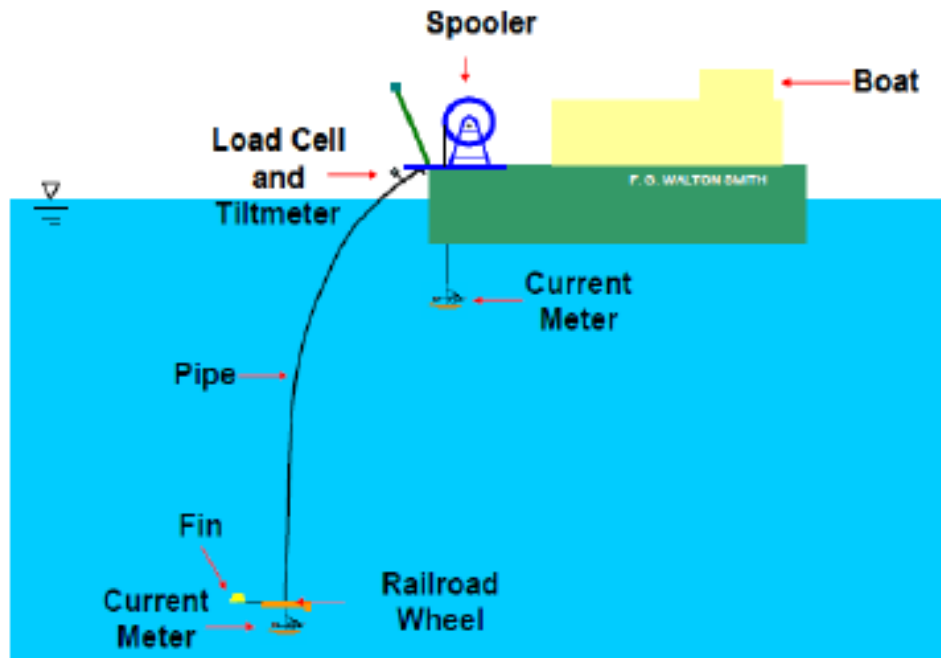


Figure 2.3. Set-up for the Gulf Stream Experiments 2006 (Jaiswal & Vandiver, 2007)

2.1.2.3 Measurement

A cross-sectional view of the pipe that is used for the experiment is shown in Figure 2.4 (Jaiswal & Vandiver, 2007). This consists of a polyethylene lining and a composite epoxy-fiber coating. During the manufacturing process, eight equal fibers were embedded into the pipe with two fibers located in every four quadrants of the pipe. To measure the VIV response, thirty-five strain gauges, with an error tolerance of one micro-strain, were included in each fiber. Every fiber has a strain gauge in every 14 feet, as shown in Figure 2.5 (Jaiswal & Vandiver, 2007). Therefore, the strain gauges from the

two fibers in the same quadrant were offset by 7 feet. The strain data were recorded at 50.4857 Hz for 180 seconds.

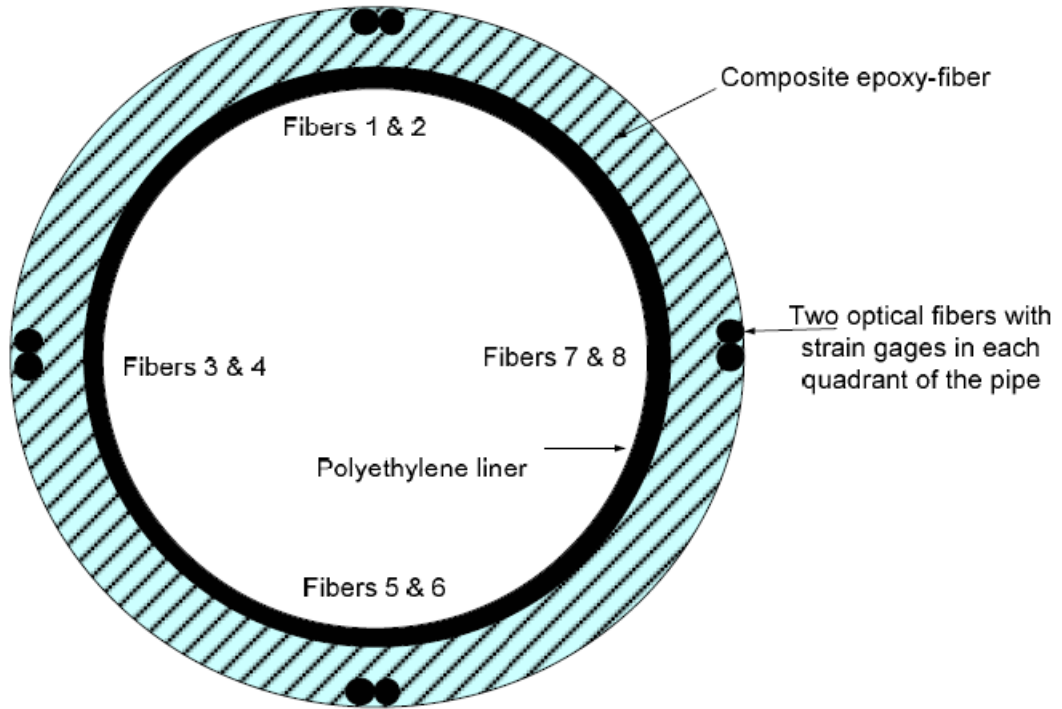


Figure 2.4. Cross-Section of the pipe from Gulf Stream test (Jaiswal & Vandiver, 2007)

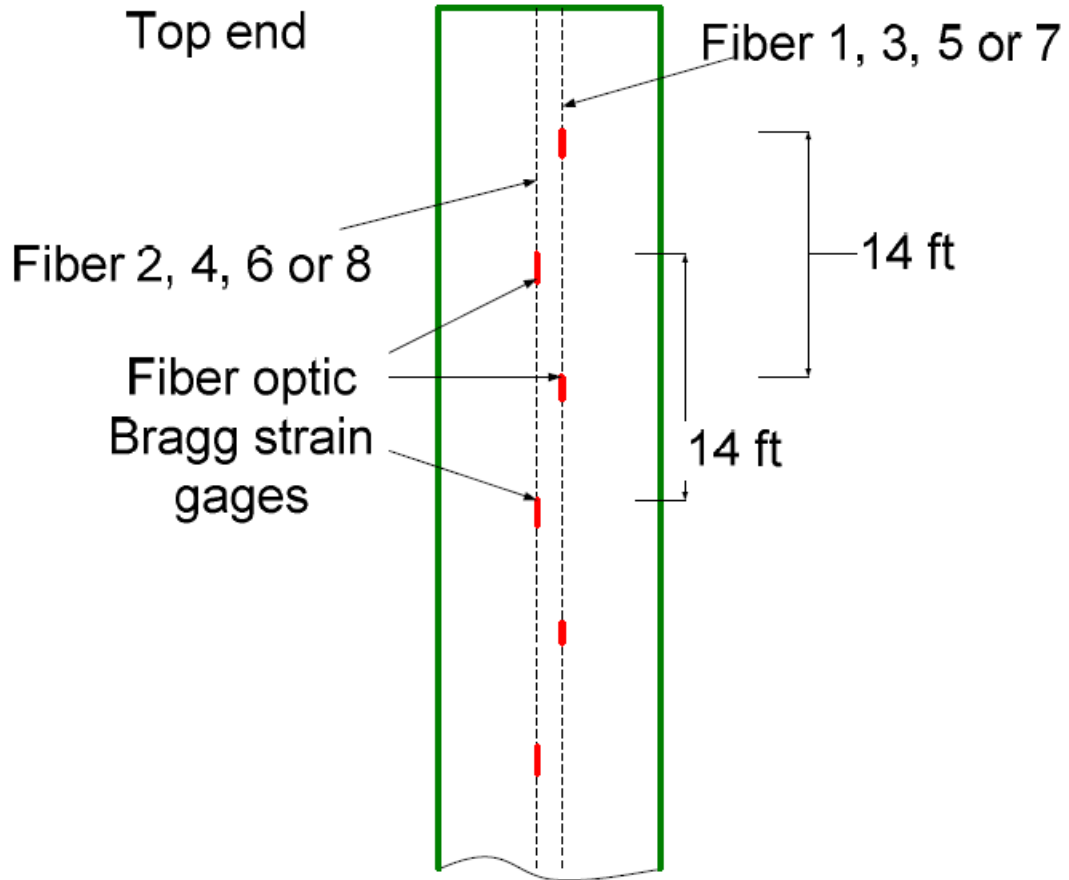


Figure 2.5. The arrangement of strain gauges in a quadrant for Gulf Stream test (Jaiswal & Vandiver, 2007)

2.2 Numerical Approach

(Newman & Karniadakis, 1997) implemented VIV of an infinitely long flexible cable was simulated with spectral element method at Reynolds numbers $Re = 100$ and $Re = 200$, corresponding to laminar and early transitional flow states, respectively. Both the standing wave and the travelling wave response is noticed. An interwoven pattern of vorticity was correlated with a standing wave cable response meanwhile a travelling wave cable response produced oblique vortex shedding. A mixed standing wave and

travelling wave cable response and chevron-like patterns with vortex shedding was came from a sheared inflow.

Huang et.al. (Huang, Chen, & Chen, 2010, 2011) conducted a simulation of VIV for a bare vertical riser using a finite-analytic Navier-Stokes (FANS) code. These authors have taken the L/D ratio as 482 in their model and results were compared with the experimental data by Lehn (Lehn, 2003) and Trim, et.al. (Trim, Braaten, Lie, & Tognarelli, 2005). Results of these simulations were in good agreement with the experimental results. The authors have reported the presence of more than one dominant modes of vibration in their simulations and these dominant modes were a function of the riser tension. According to VIV, the in-line (IL) deflection affected the cross-flow (CF).

The present research on VIV principally considered one vertical riser with fairing and presented an analytical model to estimate the instability onset conditions as the simplified two-dimensional problem (Khorasanchi & Huang, 2014). It was found that the significant role in the stability of the system was the hydrodynamic coefficients.

Many researchers focused on analyzing VIV of vertical riser with helical strakes in uniform and linearly sheared currents and predicted the vibration amplitudes and frequencies (Frank, Tognarelli, Slocum, Campbell, & Balasubramanian, 2004; Gao, Fu, Ren, Xiong, & Song, 2015; Trim, Braaten, Lie, & Tognarelli, 2005; Vandiver, Swithenbank, Jaiswal, & Marcollo, 2006) . It was reported that the maximum displacement was decreased when the strake coverage was increased (Frank et al., 2004). However, fatigue damage was not affected until the percentage of strakes coverage is reached 82% (Trim et al., 2005). The VIV responses for 40% and 70% helical strake coverage was examined and was found that 40% coverage did not create the same stress

concentration as 70%. Riser with or without strakes was tested, and the frequency and displacement response and the fatigue damage of a riser with different strakes were discussed. It was found a significant result for the fatigue damage in cross-flow (CF) and in-line (IL) direction of the bare riser. The fatigue damage in both directions is the same important parameter (Gao et al., 2015).

CHAPTER 3 METHODOLOGY

Analysis of flexible risers is inherently a multi-disciplinary problem (Ley & el Moctar, 2014). Water currents around the riser cause vortex shedding, which imparts periodic forces on the risers. These periodic forces excite different modes of deflection, which in turn changes the flow field around the risers and the resulting hydrodynamic forces. Therefore, to understand the behavior of risers in the ocean environment, a coupled fluid and structural analysis are required.

Fluid-structure interaction (FSI) problems can be analyzed in two different approaches. In the first approach, the equations that governed the fluid flows and structural behavior are cast into a set of coupled equations, and they are solved using a single program. This approach is called directly coupled approach. This approach gives very accurate results, but its time consuming and challenging to develop a coupled system. In the second approach, the governing equations for fluid flows and structural analysis are solved using well-validated independent programs and information is passed between these programs at every time step. This approach is called a loosely coupled system. One of the advantages of a loosely coupled approach is that well-validated independent legacy codes can be used for analyzing fluid flows and structural deflections. However, an interface program is needed to transfer appropriate information between these programs.

A schematic diagram of a loosely-coupled approach is shown in Figure 3.1. The geometry definition of the problem is shared between the fluid and structural solvers. The FSI analysis is started by solving the fluid dynamics equations and calculating the forces

exerted by the fluid on the structure. These forces are transferred to the structural mesh using appropriate interpolation methods. Based on these fluid forces, the structural dynamics equations are solved to get the structural deflections. The boundary surfaces of the fluid domain deflected based on the structural deflections, and the interior mesh for the fluid solver is deformed appropriately. The governing equations for fluid flows are solved again, and the newly predicted forces are transferred to the structural solver. This process is continued until a specified time is reached.

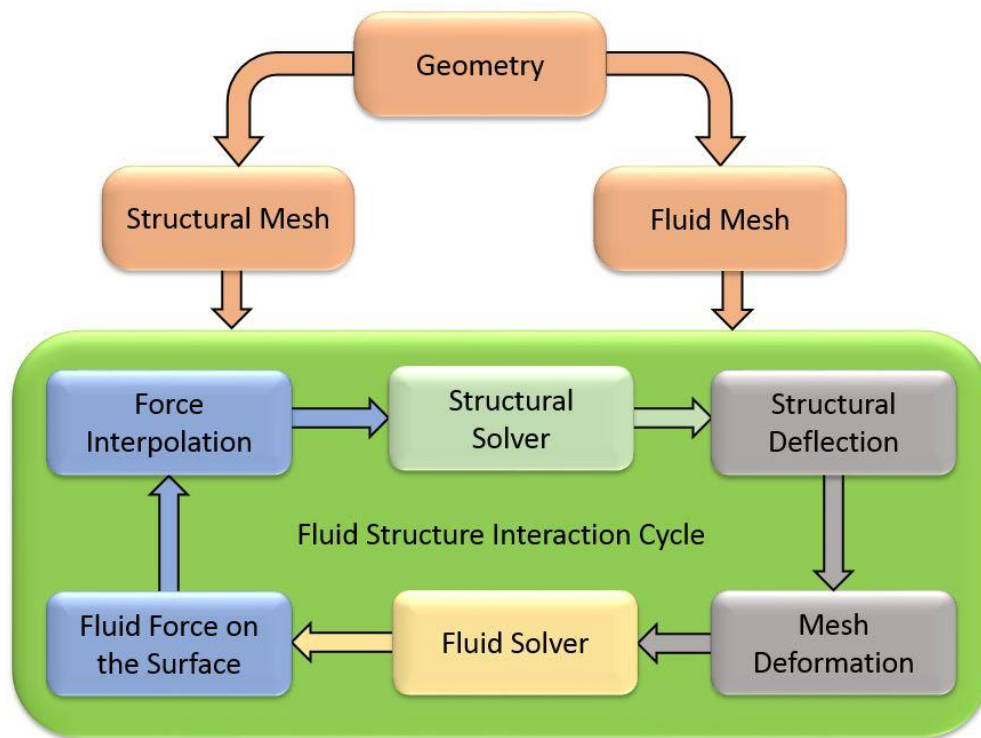


Figure 3.1. Schematic diagram of a loosely-coupled FSI approach

For the completeness, if the report, the governing equations for each of these components are listed in the following sections.

3.1 Fluid Solver

The flow around the riser is incompressible and is governed by the conservation of mass and momentum. The three-dimensional, incompressible form of these governing equations can be written as

$$\frac{\partial u}{\partial x} + \frac{\partial v}{\partial y} + \frac{\partial w}{\partial z} = 0 \quad (1)$$

$$\rho \left(\frac{\partial u}{\partial t} + u \frac{\partial u}{\partial x} + v \frac{\partial u}{\partial y} + w \frac{\partial u}{\partial z} \right) = - \frac{\partial p}{\partial x} + \mu \left(\frac{\partial^2 u}{\partial x^2} + \frac{\partial^2 u}{\partial y^2} + \frac{\partial^2 u}{\partial z^2} \right) + \rho f_x \quad (2)$$

$$\rho \left(\frac{\partial v}{\partial t} + u \frac{\partial v}{\partial x} + v \frac{\partial v}{\partial y} + w \frac{\partial v}{\partial z} \right) = - \frac{\partial p}{\partial y} + \mu \left(\frac{\partial^2 v}{\partial x^2} + \frac{\partial^2 v}{\partial y^2} + \frac{\partial^2 v}{\partial z^2} \right) + \rho f_y \quad (3)$$

$$\rho \left(\frac{\partial w}{\partial t} + u \frac{\partial w}{\partial x} + v \frac{\partial w}{\partial y} + w \frac{\partial w}{\partial z} \right) = - \frac{\partial p}{\partial z} + \mu \left(\frac{\partial^2 w}{\partial x^2} + \frac{\partial^2 w}{\partial y^2} + \frac{\partial^2 w}{\partial z^2} \right) + \rho f_z \quad (4)$$

Where t is the time, x , y , and z are the Cartesian coordinates, u , v , and w are the velocity components, μ is the dynamic viscosity, ρ is the fluid density, p is the pressure, and f_x , f_y , and f_z are the components of the body forces. (Cengel, 2010). These equations combine with the shear stress transport (SST) κ - ω turbulence model to solve them (Wilcox, 1998). The turbulence kinetic energy, κ , and the specific dissipation rate, ω , are obtained from the following transport equations.

$$\frac{\partial}{\partial t}(\rho\kappa) + \frac{\partial}{\partial x_i}(\rho\kappa v_i) = \frac{\partial}{\partial x_j} \left(\Gamma_\kappa \frac{\partial \kappa}{\partial x_j} \right) + G_\kappa - Y_\kappa + S_\kappa \quad (5)$$

$$\frac{\partial}{\partial t}(\rho\omega) + \frac{\partial}{\partial x_i}(\rho\omega v_i) = \frac{\partial}{\partial x_j} \left(\Gamma_\omega \frac{\partial \omega}{\partial x_j} \right) + G_\omega - Y_\omega + S_\omega \quad (6)$$

where G_κ and G_ω are the generation of κ and ω , respectively. Γ_κ and Γ_ω represent the effective diffusivity of κ and ω , respectively. Y_κ and Y_ω represent the dissipation of κ and ω due to turbulence. S_κ and S_ω are defined by the user.

3.2 Structural Solver

The governing equations for the structural analysis can be written as,

$$\frac{\partial^2}{\partial z^2} \left[EI \frac{\partial^2 x_i}{\partial z^2} \right] - \frac{\partial}{\partial z} \left[T \frac{\partial x_i}{\partial z} \right] + m \frac{\partial^2 x_i}{\partial t^2} + c \frac{\partial x_i}{\partial t} = F_i \quad (7)$$

where E is Young's modulus, I is the moment of inertia, T is the applied tension, m is the mass per unit length, c is the structural damping, z is the undeformed riser axis, x_1 and x_2 are the inline (IL) and cross-flow (CF) displacements, and F_1 and F_2 are the hydrodynamic forces in the IL and CF directions, respectively (Huang et al., 2011).

3.3 Modal Analysis

The modal analysis estimates the natural frequencies and mode shapes of a structure. They are essential parameters to consider when manufacturing a structure, especially if dynamic loads are encountered after installation. The equation of modal analysis can be written as

$$[M] \{ \ddot{q} \} + [C] \{ \dot{q} \} + [K] \{ q \} = \{ F \} \quad (8)$$

where q is the nodal displacement vector, and a dot shows differentiation concerning time, M is the mass matrix, C is the damping matrix, K is the stiffness matrix, and F is the hydrodynamic force vector (Chung & Hulbert, 1993).

In many riser applications and experiments, the risers are pre-stressed. The theoretical Eigen frequencies for a pre-stressed beam can be estimated using Eigen frequencies of a tensioned string and a non-tensioned beam as follows. The n^{th} Eigen frequency for the pre-stressed beam can be calculated using the relation,

$$f_{n,t-beam} = \sqrt{f_{n,string}^2 + f_{n,beam}^2} \quad (9)$$

where n is the mode number, $f_{n,string} = \frac{n}{2} \sqrt{\frac{T}{mL^2}}$ is the eigenfrequency for a tensioned string without bending stiffness and $f_{n,beam} = \frac{n^2\pi}{2} \sqrt{\frac{EI}{mL^4}}$ is the eigenfrequency for a nontensioned beam, E is Young's modulus, I is the moment of inertia, T is the applied tension, m is mass per unit length, and L is the length (Timoshenko, Young, & Weaver).

3.4 FSI Analysis using ANSYS

A schematic diagram for conducting an FSI simulation in ANSYS is shown in Figure 3.2, which involves three different components. The first one is the setup for the structural analysis, the second one is the setup for the fluid analysis, and the third one is for synchronizing the structural and fluid components. In the structural component, appropriate models that are required for the analysis of the structural behavior is selected. Additionally, the loads and constraints are also setups, and surfaces, which receive the load information from the fluid component, are also identified at this stage. In the fluid component, appropriate governing equations for the fluid flows and turbulence models for the estimation of eddy viscosity are selected. In addition, the boundary surfaces that receive displacements from the structural component are also identified in this component. The component for synchronizing the structural and fluid components is called the system coupling. In this component, the execution sequence of the fluid and structural components, time step size, time duration for the simulation, and the number of coupling iteration are set.

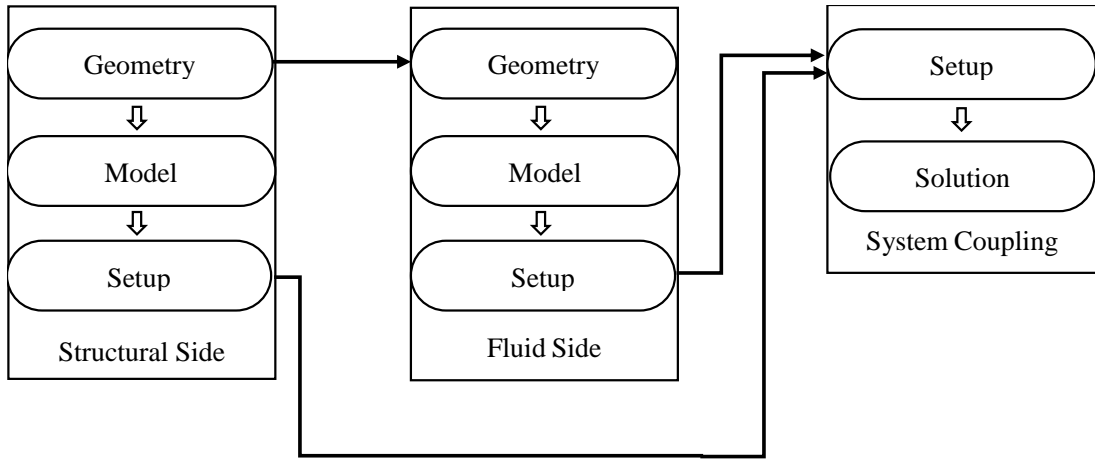


Figure 3.2. Schematic of system coupling setup in ANSYS

CHAPTER 4 RESULTS AND DISCUSSIONS

The computational approach described in Chapter 3 is validated using a VIV simulation of a flexible riser in a uniform sheared current, and the results are presented in this chapter. Different components for the FSI analysis are individually validated, before the coupled simulation. As the first step in the validation study, the dynamic behavior of the riser is analyzed using modal analysis and the computed frequencies are compared with the theoretical results. In the second step, the fluid flow around the rigid riser is simulated, and the predicted vortex shedding frequency is compared with the experimental results. These validated structural and fluid models are used for the simulation of VIV.

The geometry of the riser and the flow conditions were selected based on the experimental work by Lehn (Lehn, 2003). The flexible riser used in this experiment has a length-to-diameter ratio (L/D) of 481.5 and mass ratio of 0.7 kg/m. The riser has a wall thickness of 0.045 mm and the external diameter of 20 mm. The different parameters of the riser model used in the experiment are summarized in Table 7. For the simulation, the structural damping is set to zero, a tensile force of 817 N is applied on the top of the riser, and the top and bottom of the riser are modeled as fixed support. The approach velocity of the fluid is taken as is 0.2 m/s, which corresponds to experiment 1103 by Lehn. The numerical results from the computations are compared with the experimental data (Lehn, 2003) in the following sections. Also, the optimum number of processors needed to

reduce the overall simulation time is carried out using simulations with a different number of processors, and the results are presented in this chapter.

Properties	Values	Units
L	9.63	m
D	20	Mm
t_w	0.45	Mm
E	1.025×10^{11}	N/m ²
T	817	N
m^*	0.7	kg/m

Table 7. The properties of the riser model used

4.1 Modal Analysis

The geometry of the riser described above, see Figure 4.1, is discretized using Mesher in ANSYS for modal and structural analyses. The number of divisions along the circumferential direction is set as 20 using the option edge sizing, the number of divisions in the radial direction is set as default, and the number of divisions along the axial direction is set as 250 using the options face meshing in Mesher. The resulting mesh for the riser is shown in Figure 4.2.

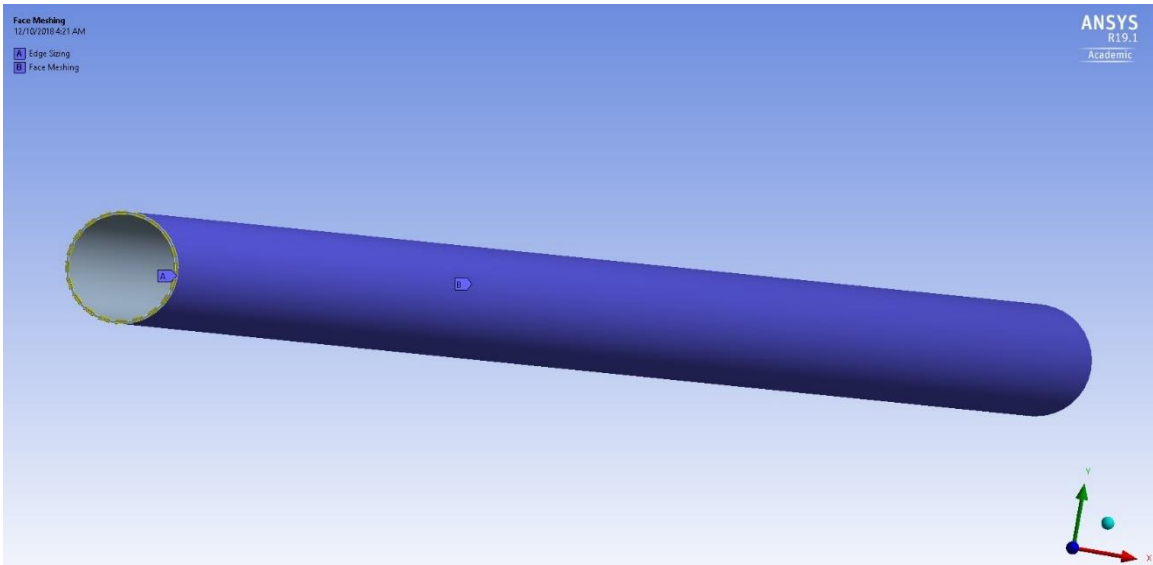


Figure 4.1. The geometry of the riser

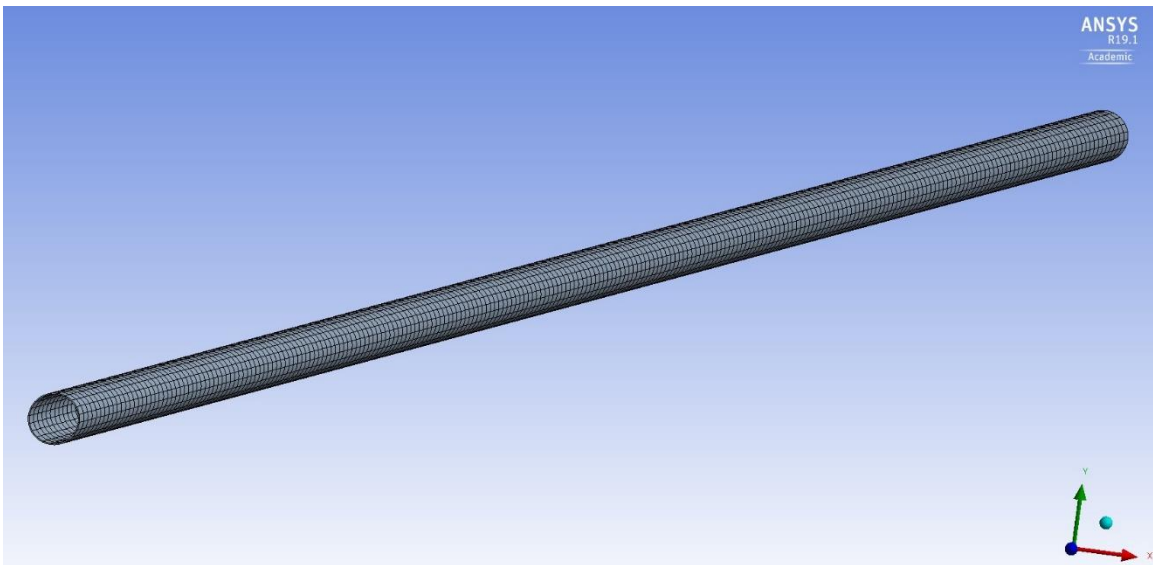


Figure 4.2. The mesh on the riser

The Eigen frequencies of the first eight modes are simulated with a modal analysis performed using ANSYS. To mimic the tension applied to the riser in the experimental work, a pre-stressed model is used in the modal analysis. For this purpose, a static structural analysis is carried out using a specified tension, the computed stresses are saved to a file, and these stresses are read into the modal analysis as the initial condition.

For the static structural analysis, the following boundary conditions are used. 1) Remote displacement boundary condition is applied on bottom face, X, Y, Z components of displacement are set zero. Remote displacement boundary condition is applied on top face, and the X and Y components of displacements are set to zero while Z component of displacement is set to free. Also, the rotation with respect to the X- and Y-axes are set as free for the bottom and top surfaces, while rotation with respect to the Z-axes is set as zero. 2) A tensile force of magnitude is 817 N applied on the top face. After the structural analysis, the command “inistate,write,1,,,,,s” is used to export the stress to an external file.

For the modal analysis, remote displacement boundary condition is applied on the bottom, and top faces and the X, Y, Z components of the displacement and rotation with respect to the Z-axis are set to zero. Also, the rotation with respect to the X- and Y-axes are set as free. The command “inistate,read,file,ist,’file location” is used to read the stress information that is saved from the static structural analysis and set pre-stress information. The Eigen frequencies from the simulation are compared with the theoretical results in Table 8. The theoretical values of the Eigen frequencies were calculated using equation (9) in Chapter 3. As given in the table, each mode has two frequencies, one for the vibration along the in-line (IL) direction and the other in the cross-flow (CF) direction. However, the magnitude of these two frequencies is almost the same. The values of Eigen frequencies are good agreement with theoretical values, with a maximum error of 0.1008%.

Mode	$f_{n, \text{ string}}$ (Hz)	$f_{n, \text{ beam}}$ (Hz)	Theoretical Value (Hz)	Direction	FEA (Hz)	Error
1	1.77	0.24	1.79	IL	1.7907	0.0391%
				CF	1.7911	0.0615%
2	3.55	0.94	3.67	IL	3.6736	0.0981%
				CF	3.6737	0.1008%
3	5.32	2.12	5.73	IL	5.7327	0.0471%
				CF	5.7328	0.0489%
4	7.1	3.77	8.04	IL	8.04	0%
				CF	8.0401	0.0012%
5	8.87	5.89	10.65	IL	10.653	0.0282%
				CF	10.653	0.0282%
6	10.64	8.48	13.62	IL	13.615	0.0367%
				CF	13.615	0.0367%
7	12.42	11.55	16.96	IL	16.959	0.0059%
				CF	16.959	0.0059%
8	14.2	15.08	20.71	IL	20.708	0.0097%
				CF	20.708	0.0097%

Table 8. Eigen frequencies for the flexible riser

4.2 Fluid Flow Analysis

The computational domain for the fluid flow analysis is shown in Figure 4.3. The origin of the computational domain is located at the center of the bottom end of the riser, see Figure 4.3. This region consists of 200 mm (10D) upstream and sides, 600 mm (30D) downstream and 9.63 m (481.5D) along the axial direction.

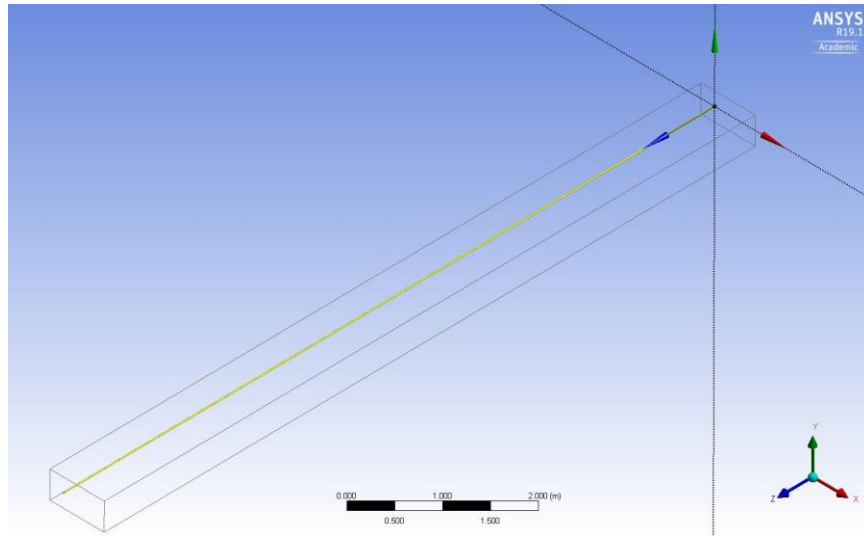


Figure 4.3. Computational domain for fluid flow analysis

The computational domain is discretized using a multi-block approach for the simulation, and Figure 4.4 shows the top view of the block structure used for the discretization of the computational domain. Using the edge sizing option in Mesher, the number of divisions for the segments A, B, C, D, E, and F are set as 180, 45, 60, 20, 40 and 10 respectively, as shown in Figure 4.5. For the boundary layer mesh, the distance of the first layer of the mesh from the riser surface is set as 0.00001 m, and maximum layers in the boundary layer mesh are set as 24. The mesh in the top plane and a zoomed view of the mesh around the riser are shown in Figure 4.6 and Figure 4.7, respectively. A coarse mesh and a fine mesh are generated by extruding the mesh on the top plane by the different number of divisions along the axial direction. The number of divisions along the axial direction for coarse mesh and fine mesh is set as 20 and 40, respectively. This resulted in a number of elements for the coarse mesh 415200, and for fine mesh 830400. These meshes are shown in Figure 4.8 and Figure 4.9, respectively.

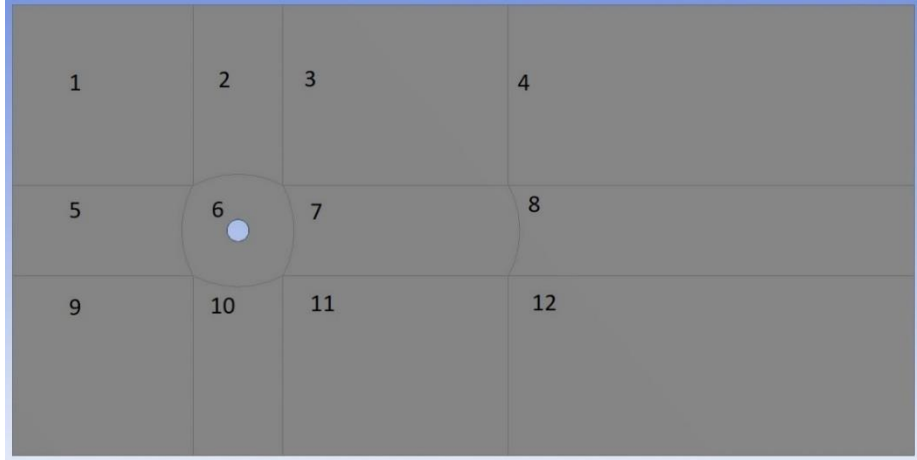


Figure 4.4. Block structure on top XY-plane

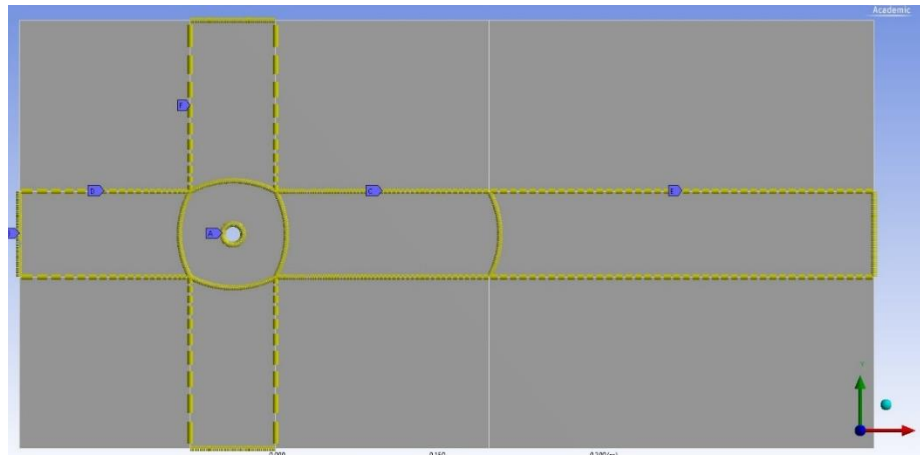


Figure 4.5. The number of divisions on the selected boundary segments

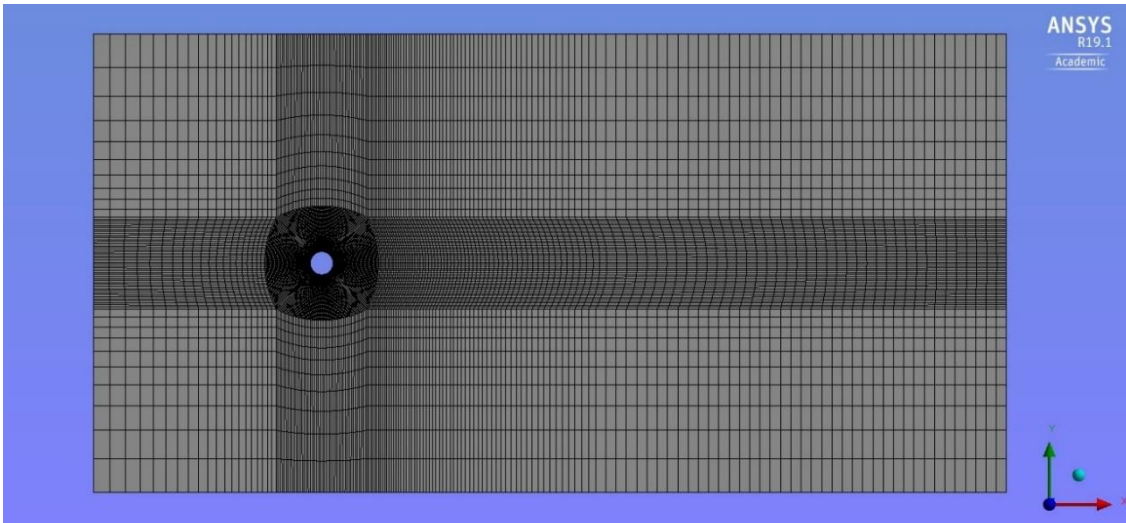


Figure 4.6. Mesh on top XY-plane

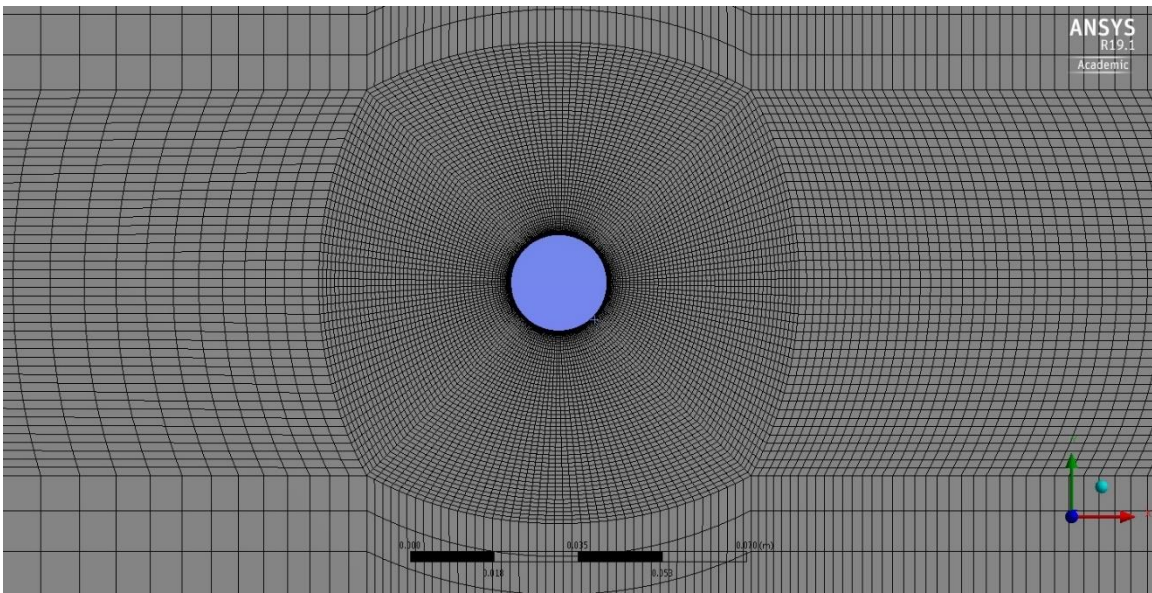


Figure 4.7. Mesh around the riser



Figure 4.8. Overall view of the coarse mesh

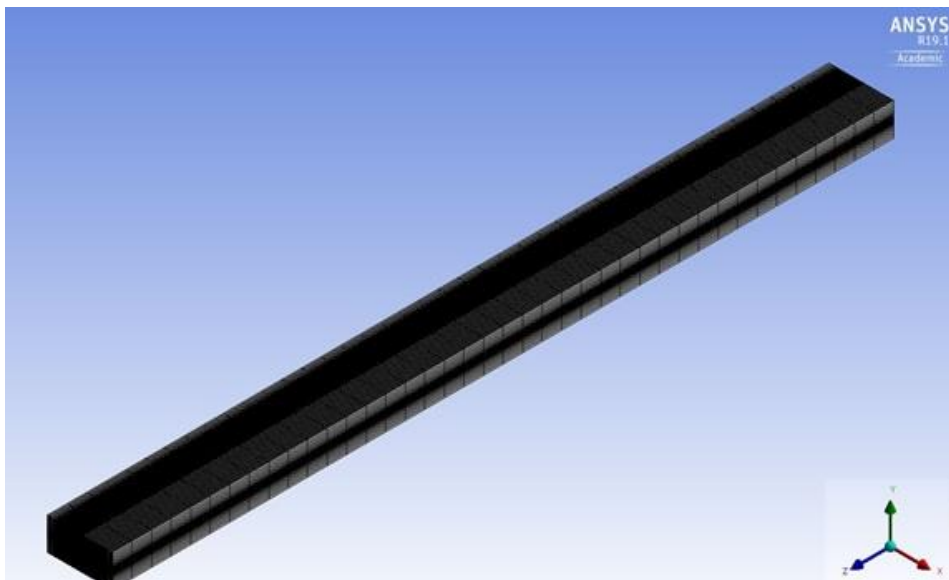
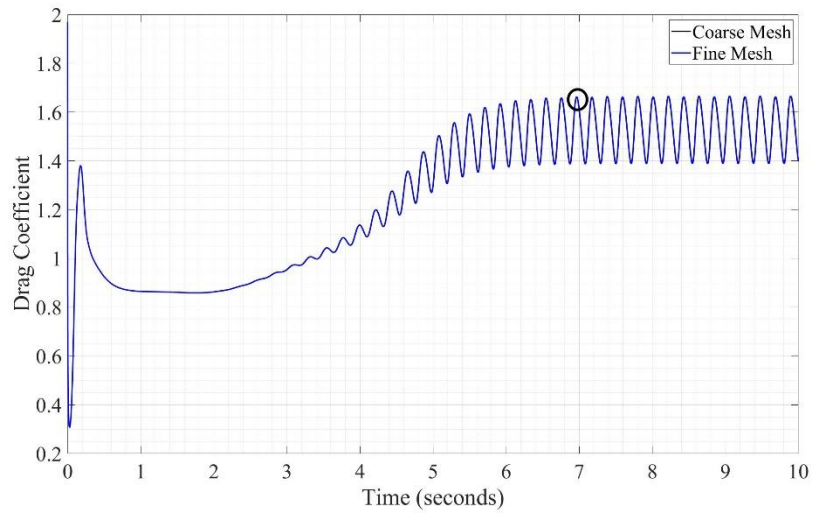


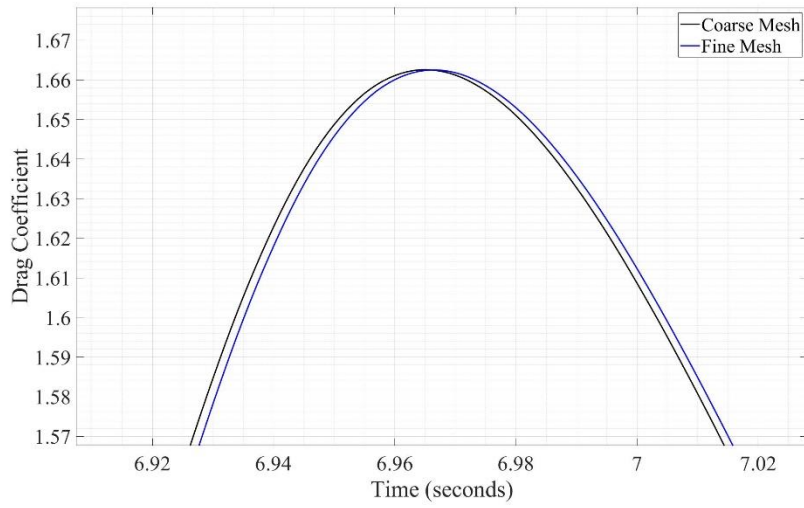
Figure 4.9. Overall view of the fine mesh

The incompressible form of the Navier-Stokes equations, given in Chapter 3, is taken as the governing equation for the fluid flow and the eddy viscosity is estimated using the SST κ - ω turbulence model. For the unsteady simulations, the time step size is set as 0.001 s, and the number of iterations as 10000. To resolve the unsteady flow

accurately, a maximum of 20 sub-iterations are used in each time. Flow simulations are carried out for uniform velocities of 0.2 m/s and 0.42 m/s. The time history of the drag coefficient for the coarse and the fine mesh at velocities 0.2 m/s and 0.42 m/s are shown in Figure 4.10 and Figure 4.14, respectively. Similarly, the time history of the lift coefficient for the coarse and the fine mesh at velocities 0.2 m/s and 0.42 m/s, are illustrated in Figure 4.12 and Figure 4.16, respectively. These plots show the periodic vortex shedding is established approximately around 7 seconds. A Fourier analysis of the time history of lift and drag is used to calculate the vortex shedding frequency and the Strouhal number. Fourier analysis is conducted using MATLAB, and the data from initial transients are neglected for these calculations. The power-spectral frequency of the drag coefficient and the lift coefficient for the freestream velocity of 0.2 m/s are shown in Figure 4.11 and Figure 4.13, respectively. Similar plots for a freestream velocity is 0.42 m/s are shown in Figure 4.15 and Figure 4.17, respectively. The zoomed-in region of the maximum power-spectral density in these graphs verifies that the coarse and the fine meshes predict the same vortex shedding frequency. This is because the flow is essentially 2-dimensional since the riser is considered as a rigid body and the mesh remains the same at different axial locations.

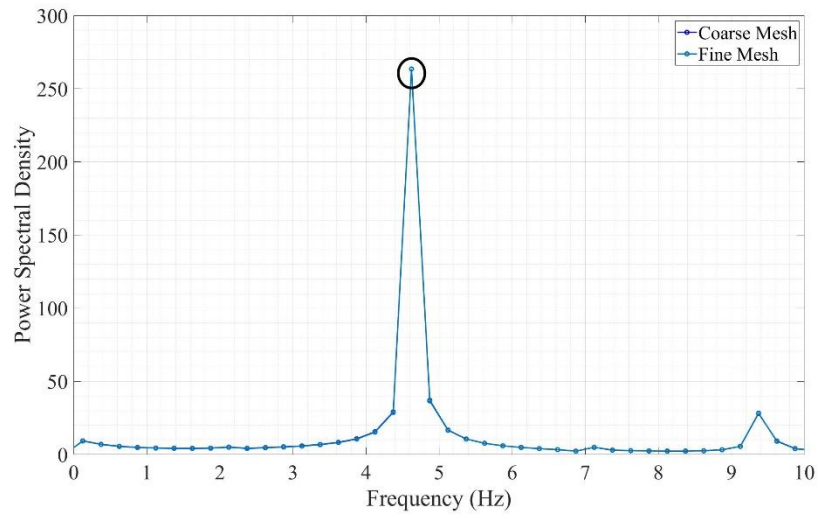


(a) Overall view

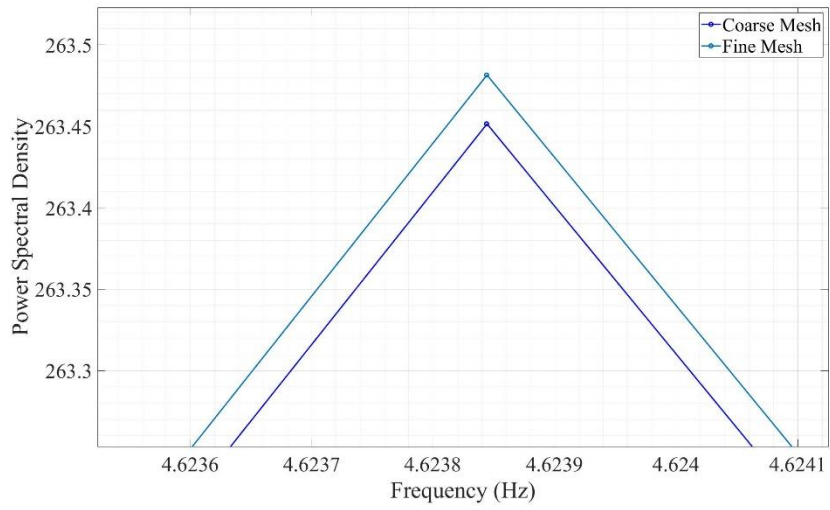


(b) Zoomed in view

Figure 4.10. Drag history for the flow with a freestream velocity of 0.2 m/s

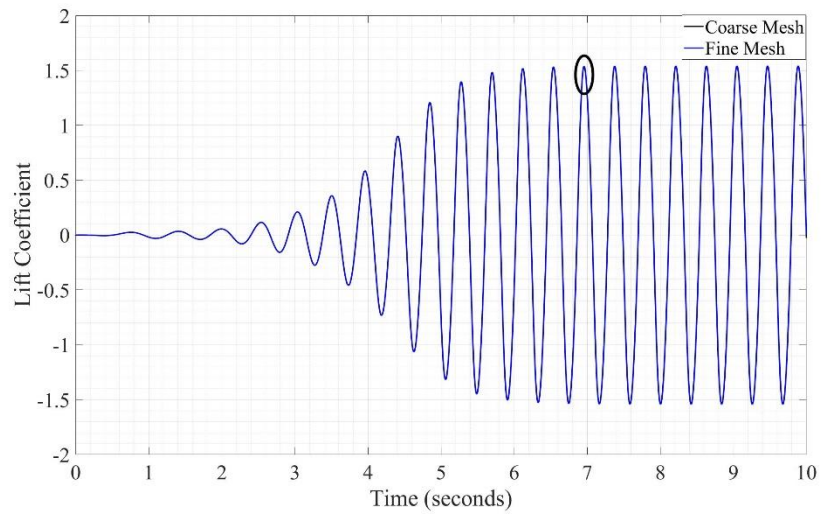


(a) Overall view

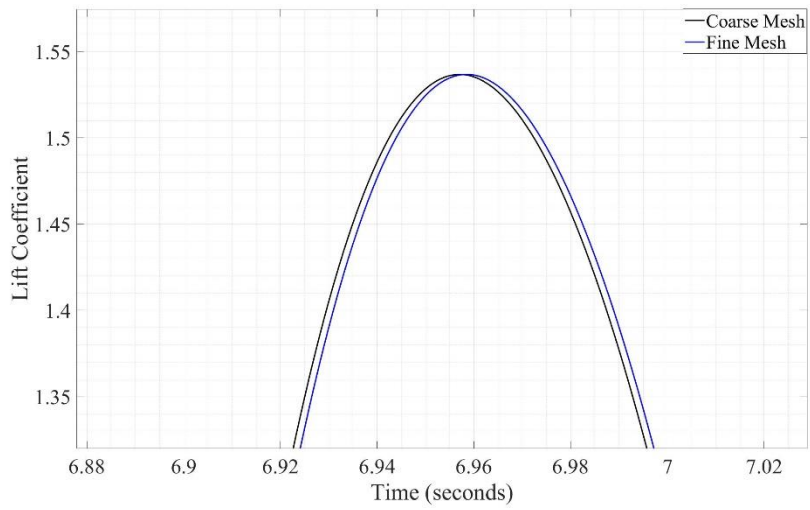


(b) Zoomed in view

Figure 4.11. Power spectral density from drag history for the flow with a freestream velocity of 0.2 m/s

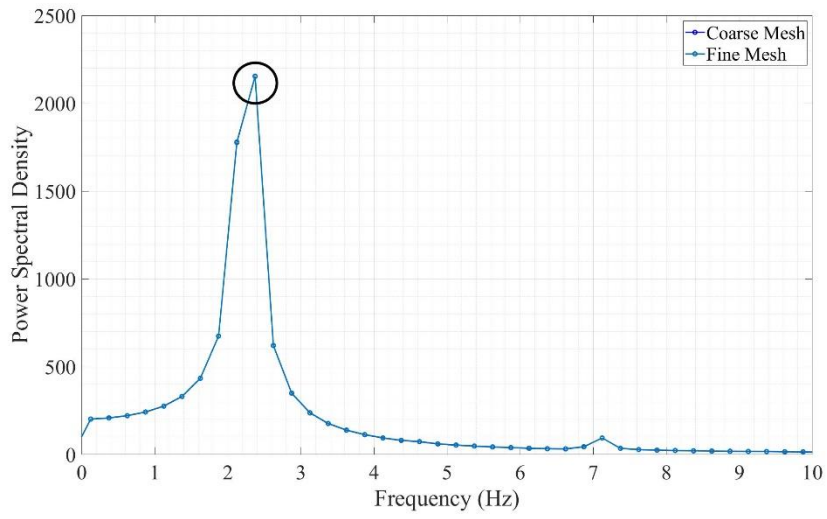


(a) Overall view

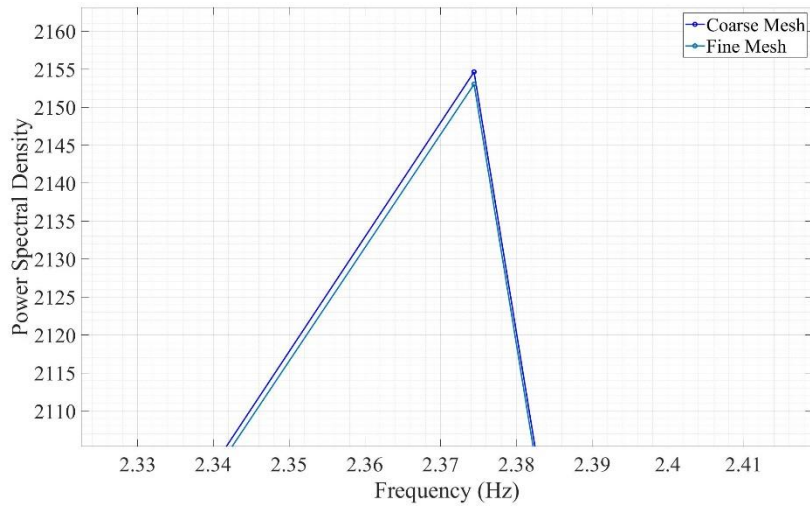


(b) Zoomed in view

Figure 4.12. Lift history for the flow with a freestream velocity of 0.2 m/s

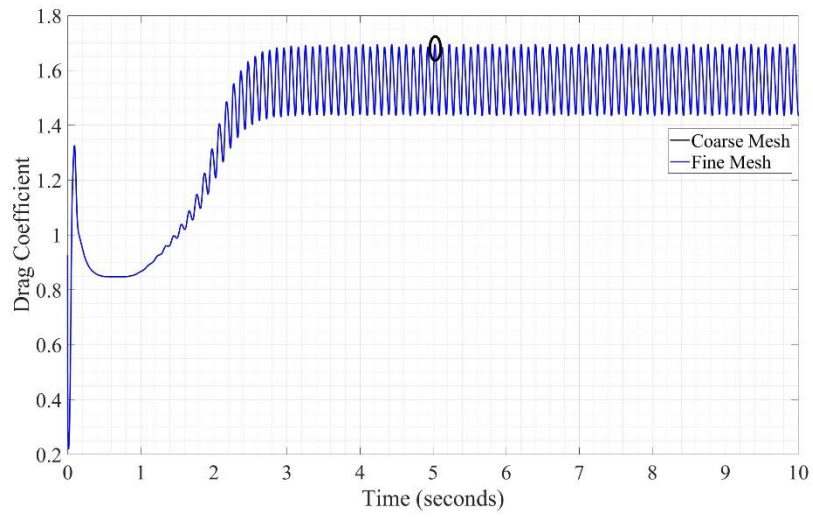


(a) Overall view

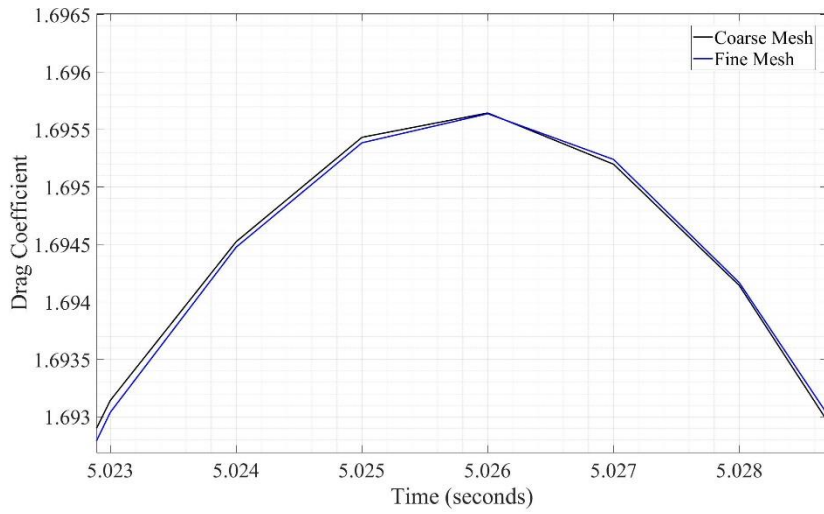


(b) Zoomed in view

Figure 4.13. Power spectral density from lift history for the flow with a freestream velocity of 0.2 m/s

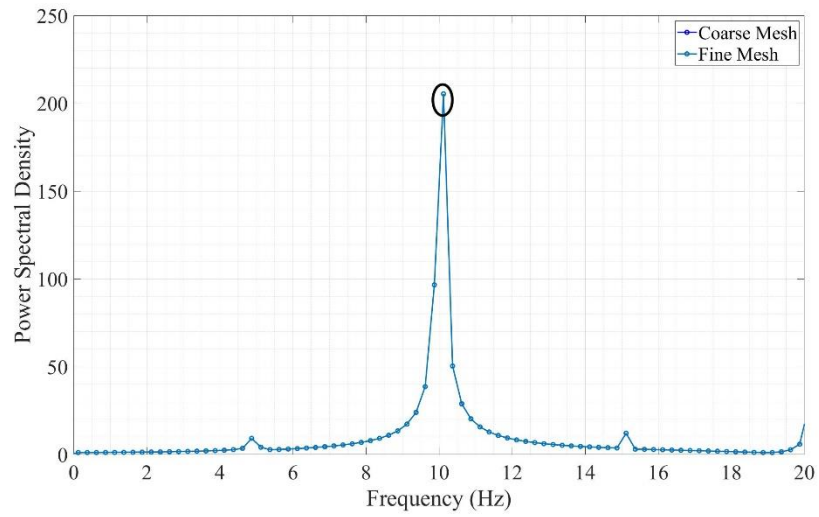


(a) Overall view

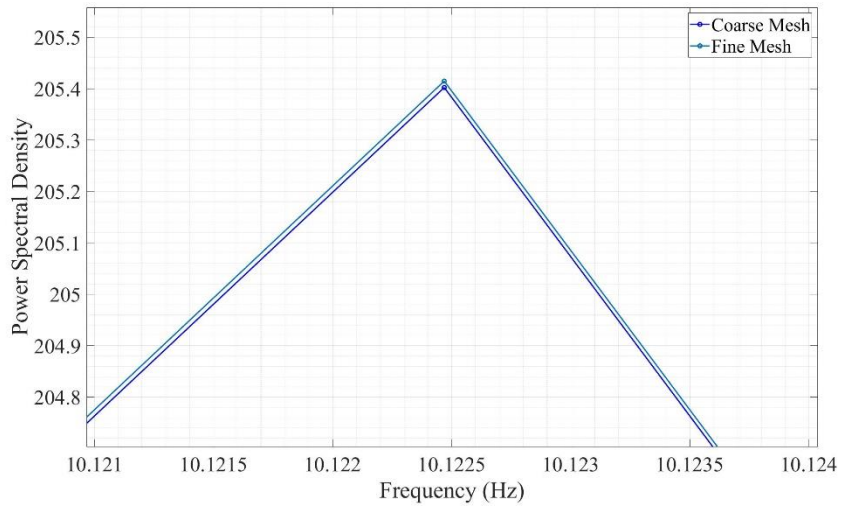


(b) Zoomed in view

Figure 4.14. Drag history for the flow with a freestream velocity of 0.42 m/s

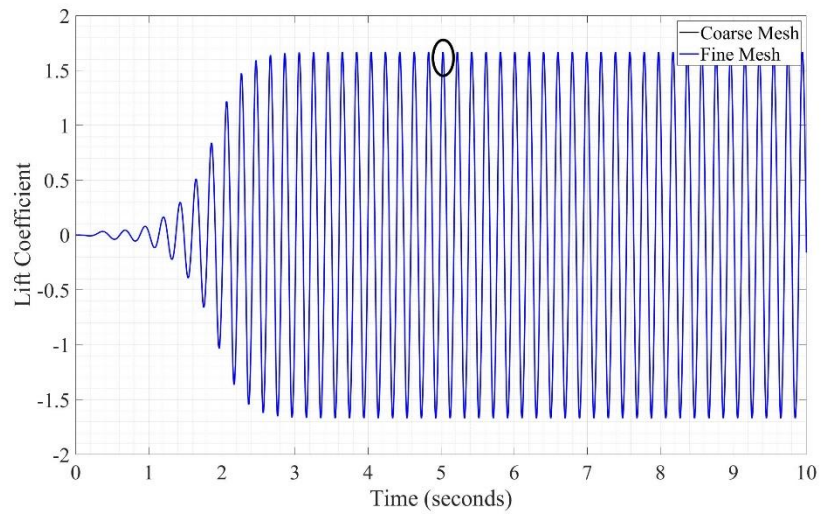


(a) Overall view

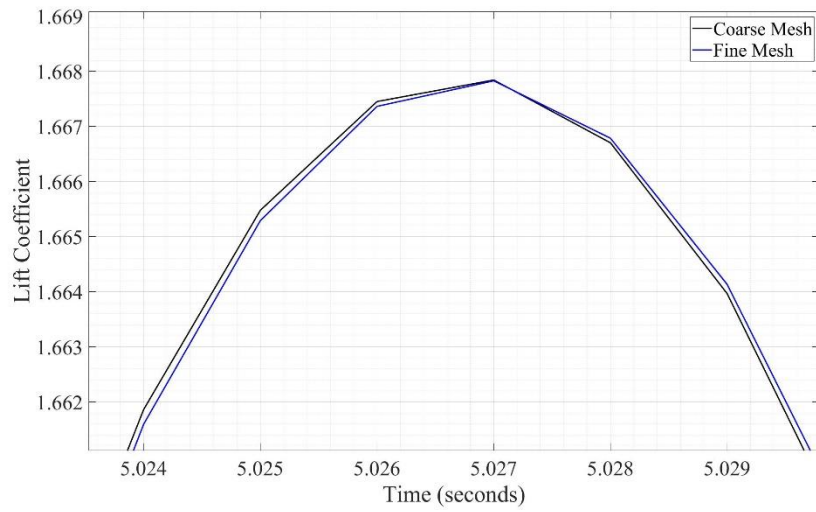


(b) Zoomed in view

Figure 4.15. Power spectral density from drag history for the flow with a freestream velocity of 0.42 m/s

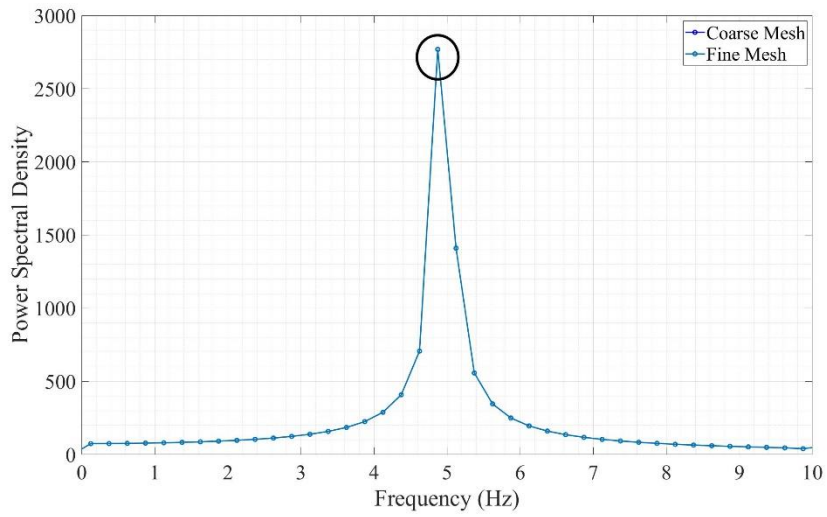


(a) Overall view

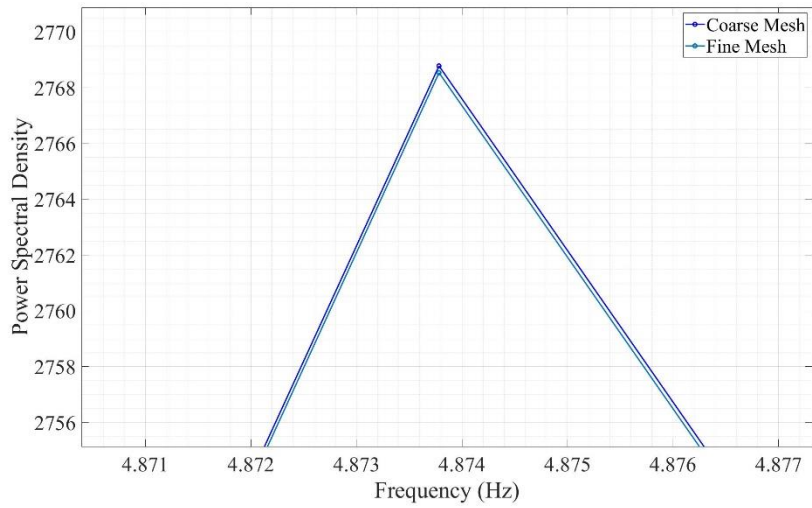


(b) Zoomed in view

Figure 4.16. Lift history for the flow with a freestream velocity of 0.42 m/s



(a) Overall view



(b) Zoomed in view

Figure 4.17. Power spectral density from lift history for the flow with a freestream velocity of 0.42 m/s

The vortex shedding frequencies and the corresponding Strouhal numbers are summarized in Table 9. It can be seen from the table that the Strouhal number the drag is

twice as the one from the lift. This is due to the fact that during each oscillation two vortices of equal magnitude, but opposite signs are shed from the cylinder. The drag force acting on the cylinder is a function of the sign of the vortex, while the lift force is not a function of the sign of the vortex. Therefore, the Strouhal number from the lift force is typically used for the comparison with the experimental data. The Strouhal number is a function of the Reynolds number, and it varies between 0.2 and 0.4. For the Reynolds number used in this analysis, the Strouhal number is approximately 0.22 (Taylor, Nudds, & Thomas, 2003). The Strouhal number computed from the lift coefficient at velocities are 0.2 m/s, and 0.42 m/s are 0.237 and 0.232, respectively, which agrees well with the experimental values. The velocity distribution at a constant axial cross-section, for velocities 0.2 m/s and 0.42 m/s, showing the vortex shedding is shown in Figure 4.18, Figure 4.19, Figure 4.20 and Figure 4.21. These computations took approximately 13 hours for the coarse and approximately 18 hours for the fine mesh using 8 processors and 2048 RAM.

Diameter [m]	0.02			
Velocity [m/s]	Reynolds Number	According to	Frequency	Strouhal Number
0.2	3980.857	Drag Coefficient	4.62	0.462
		Lift Coefficient	2.37	0.237
0.42	8359.801	Drag Coefficient	10.12	0.482
		Lift Coefficient	4.87	0.232

Table 9. Frequency and Strouhal number from fluid flow analysis

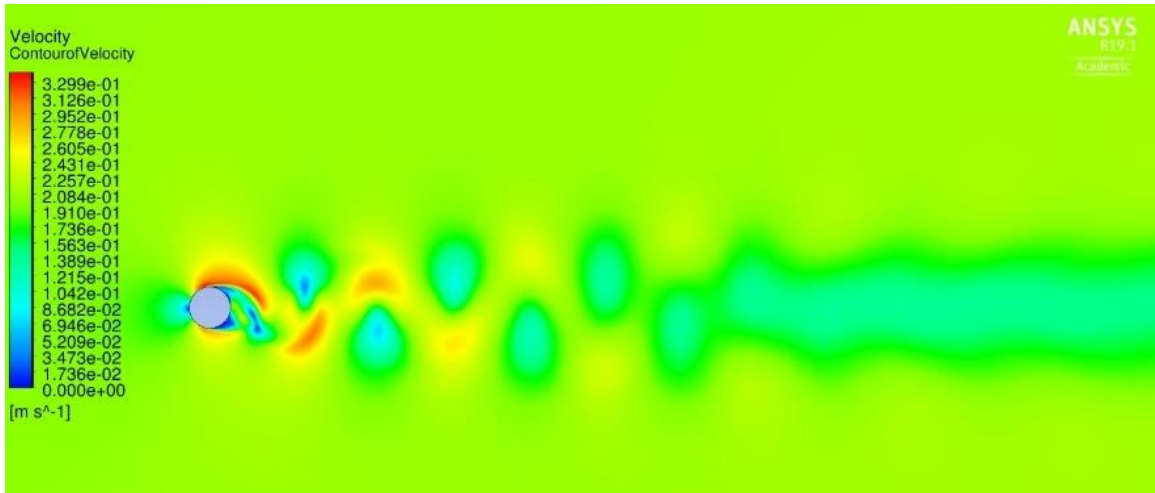


Figure 4.18. Vortex shedding at $z/L = 0.22$ of the riser at freestream velocity, 0.2 m/s, on the coarse mesh

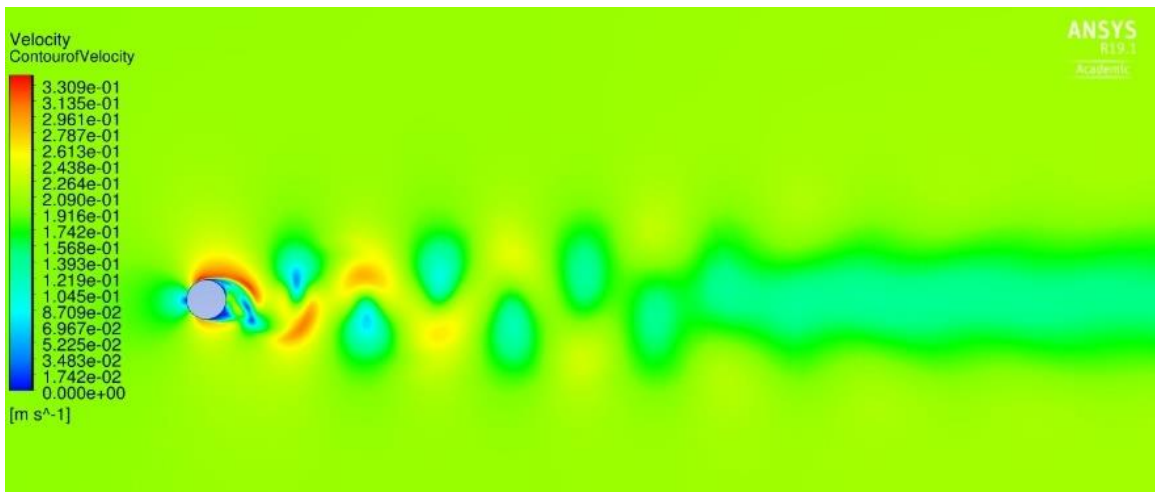


Figure 4.19. Vortex shedding at $z/L = 0.22$ of the riser at freestream velocity, 0.2 m/s, on the fine mesh

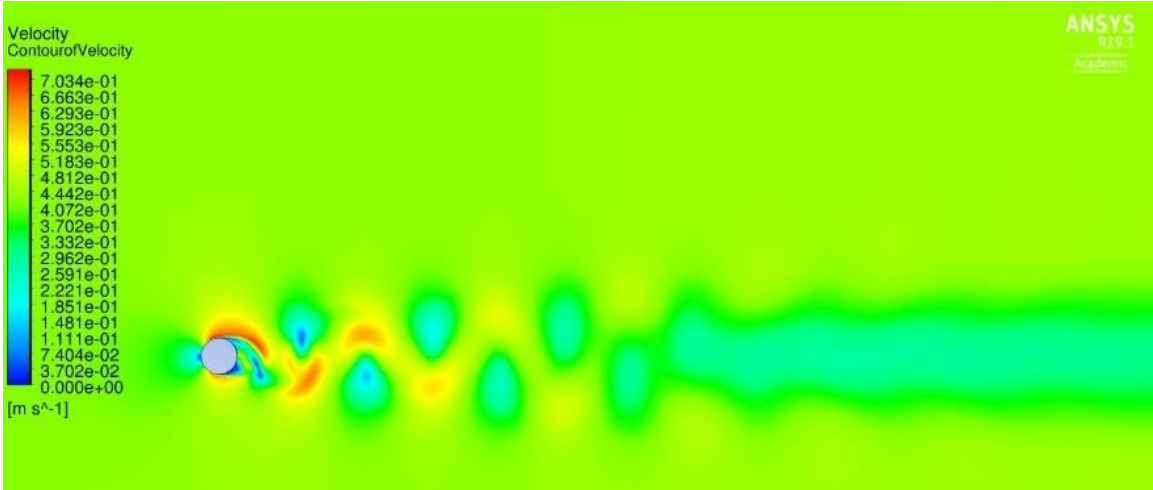


Figure 4.20. Vortex shedding at $z/L = 0.22$ of the riser at freestream velocity, 0.42 m/s, on the coarse mesh

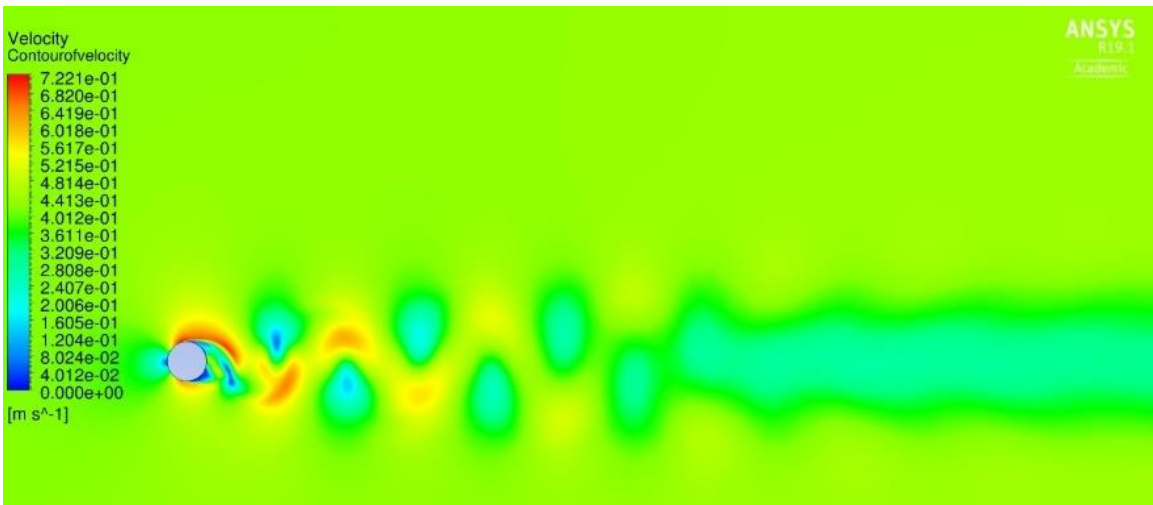


Figure 4.21. Vortex shedding at $z/L = 0.22$ of the riser at freestream velocity, 0.42 m/s, on the fine mesh

4.3 Estimation of Speed-up and the Number of Processors

Fluid-structure interaction (FSI) analysis is computationally very expensive. Therefore, it is essential to use an appropriate number of processors to reduce the wall clock time. Each computer node of the Linux cluster used for the simulation has 24

processors, and the simulations are carried out in an interactive mode using a single compute node. To select an optimum number of processors for the fluid analysis, the number of processors for the mechanical solver is fixed, and the number of processors for the fluid solver is varied and the timesaving is calculated by comparing the CPU time with the time need for one processor. For this comparison, only 10 iterations for the FSI analysis is considered. This time saving for the different number of processors is plotted in Figure 4.22. The Y axes is the speed up defined as the ratio of the time taken by the given number of processors and the time taken by a single processor. The best time saving is obtained when the number of processors is 22.

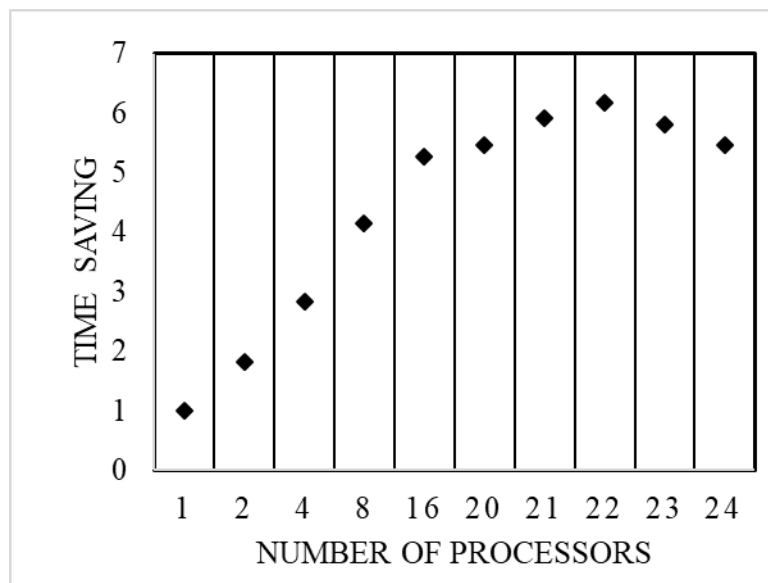


Figure 4.22. Speed-up obtained when using a different number of processors for the fluid solver

A similar step is used to find the optimum number of processors needed for the mechanical solver. In this case, the number of processors for the fluid solver is set as 22 and the number of processors for the mechanical solver is varied, and the speed-up is estimated. Figure 4.23 shows the speed-up when the number of processors for the

mechanical solver is varied, and it can be seen that the best time saving obtained for 8 processors. Therefore, for the FSI analysis, 22 processors were used for the fluid solver and 8 processors were used for the structural solver.

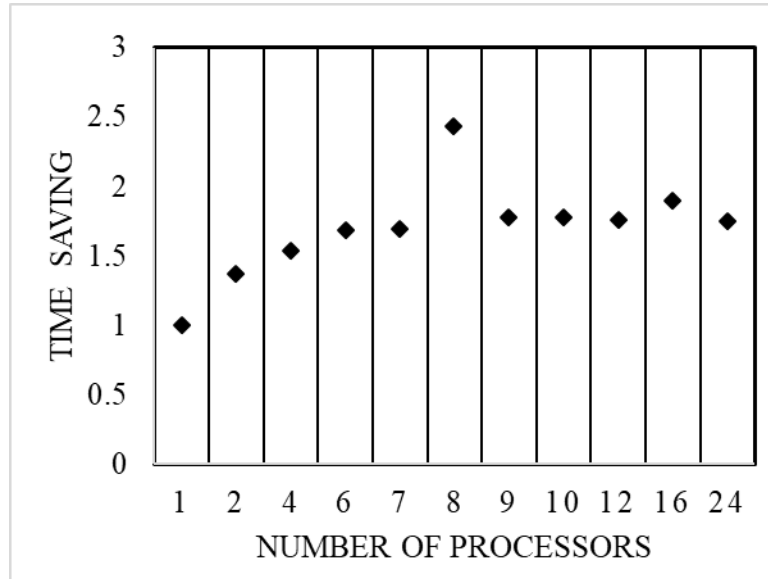


Figure 4.23. Speed-up obtained when using a different number of processors for the structural solver

4.4 Convergence of the Fluid and FSI Analyses

Temporal accuracy for simulations in ANSYS is achieved using multiple iterations during every time step. It is important to ensure convergence of the fluid and FSI analyses during these iterations at every time step to get time accurate results. Figure 4.24 and Figure 4.25 show the residual histories of fluid analysis and FSI analysis respectively for a few time steps. It can be seen from these figures that solvers convergence well during each time step.

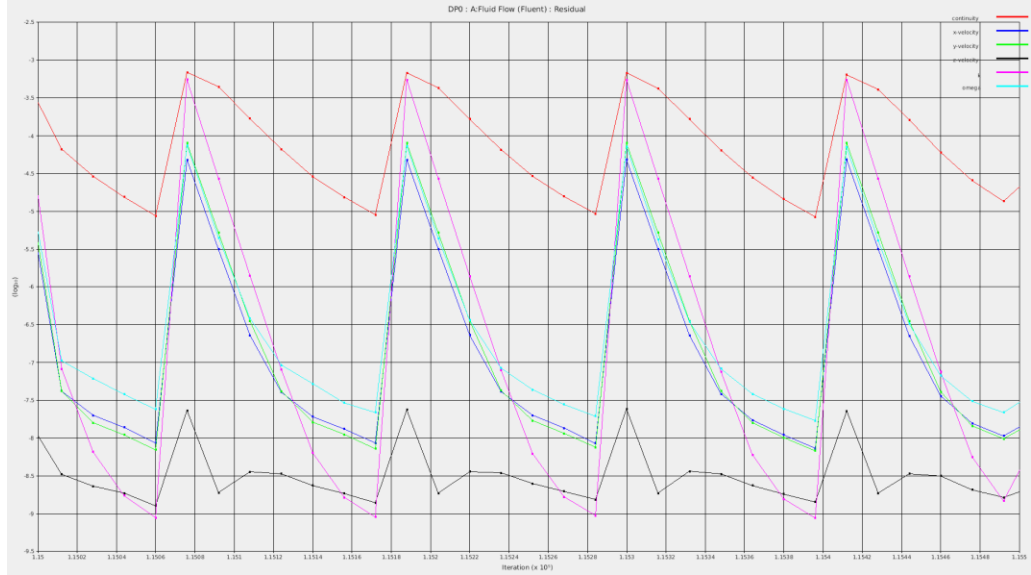


Figure 4.24. The residual of the fluid analysis

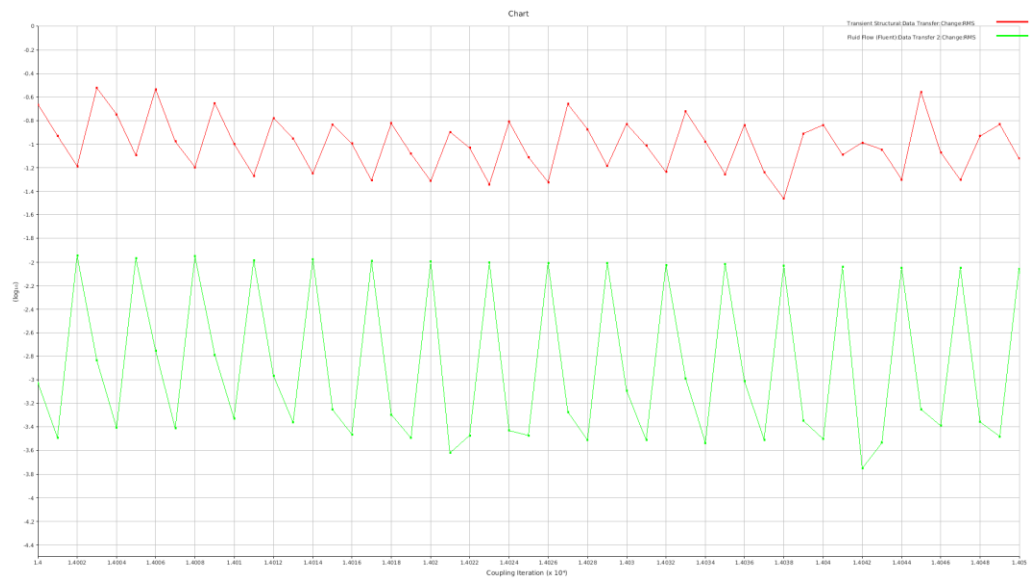


Figure 4.25. The residual of the FSI analysis

4.5 Results from FSI Analysis and Comparison with the Experimental Data

The FSI analysis of the flexible riser is carried out using the steps described in Section 3.4 of Chapter 3. Three different simulation components (Transient structural, Fluid Flow, and System Coupling) from ANSYS Workbench are used for this analysis.

Setup in Transient Structural and Fluid Flow is linked with Setup in System Coupling, as shown in Figure 4.26. The common boundary representing the outside surface of the riser is used for transferring load information from the fluid side to the structural side, and the deflection information from the structural side to the fluid side. This data transfer is setup in System Coupling. Appropriate boundary conditions for these surfaces are also setup in Transient Structural and Fluid Flow components. Also, the solution in Transient Structural is linked with Results in Fluid Flow to visualize the results from the structural analysis and fluid flow together.

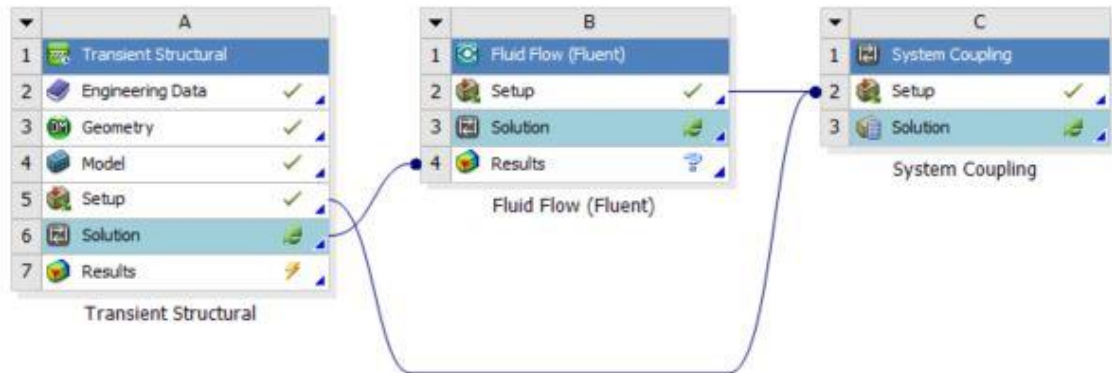


Figure 4.26. Schematic diagram of the system coupling in ANSYS

These analyses were performed for a uniform sheared current with two different meshes, the coarse and the fine meshes presented earlier. To save the computational time, the results from the unsteady fluid flow simulations is used as the initial conditions for the FSI analysis. In this analysis, time step size and the duration of the analysis were set as 0.0008 s and 4 s, respectively. The maximum iterations per time step for the system coupling, the structural solver, and the fluid solver were set as 3, 3 and 5, respectively. The computational time taken for this analysis using the coarse mesh at the velocity of

0.2 m/s, was approximately 80 hours, while for fine mesh at the same velocity the computational time taken was approximately 102 hours. Similarly, for the freestream velocity of 0.42 m/s, the time taken for coarse mesh and the fine meshes were approximately 94 hours and 112 hours respectively.

The computed in-line (IL) and cross-flow (CF) vortex induced vibrations are compared with the experimental data by Lehn (Lehn, 2003) below. For a freestream velocity of 0.2 m/s, the root mean square (RMS) amplitudes of vibrations in the IL and CF directions are shown in Figure 4.27 and Figure 4.28, respectively. In these plots, the experimental data are plotted as black circles. The results from the fine mesh and coarse mesh are in good agreement with experimental data. The RMS values of vibration along IL and CF directions for the last five cycles of oscillations from the coarse and fine meshes are plotted in Figure 4.29, Figure 4.30, Figure 4.31 and Figure 4.32. It can be seen from these figures that the scattering of the data is much smaller for the fine mesh as compared with the coarse mesh. The maximum IL and CF RMS amplitude in the fine mesh are approximately 0.115 and 0.447, and the location of maximum IL amplitude is at $z/L = 0.22$ whereas maximum CF amplitude is at $z/L = 0.44$.

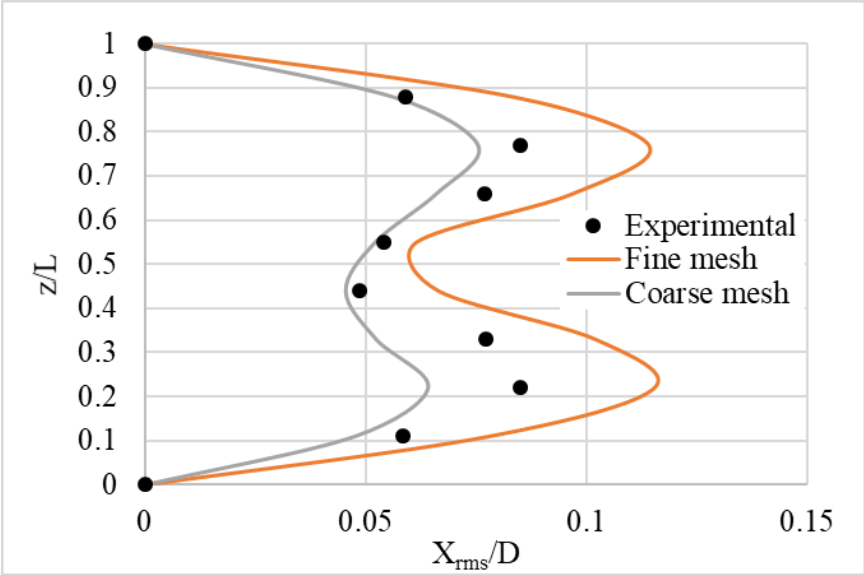


Figure 4.27. Comparison of the RMS amplitudes in IL direction between fine and coarse mesh systems with published data at freestream velocity = 0.2 m/s

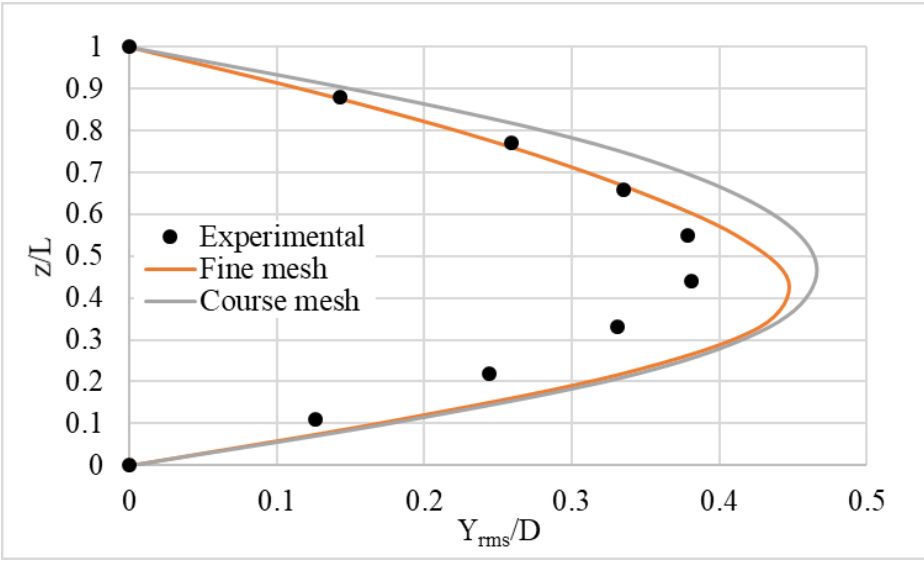


Figure 4.28. Comparison of the RMS amplitudes in CF direction between fine and coarse mesh systems with published data at freestream velocity = 0.2 m/s

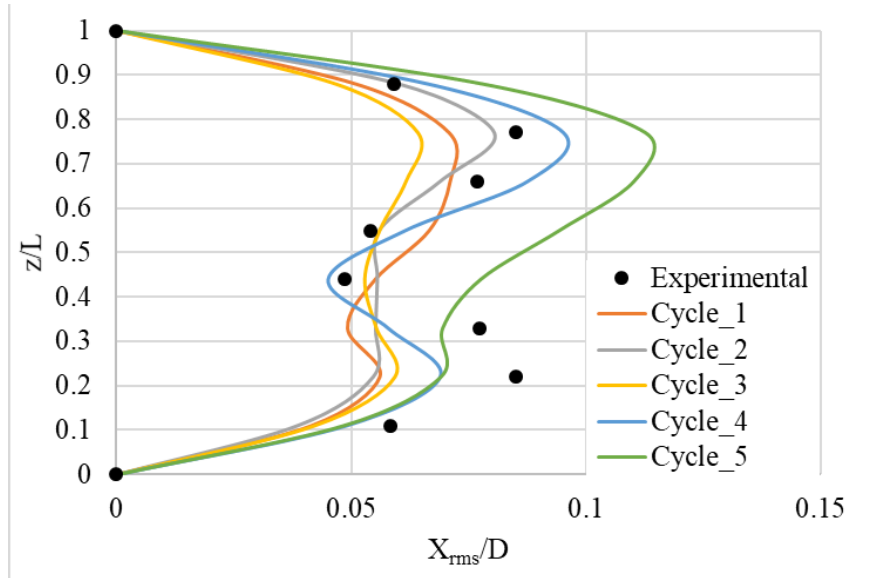


Figure 4.29. Comparison of data from difference oscillation cycles in in-line (IL) direction on the coarse mesh

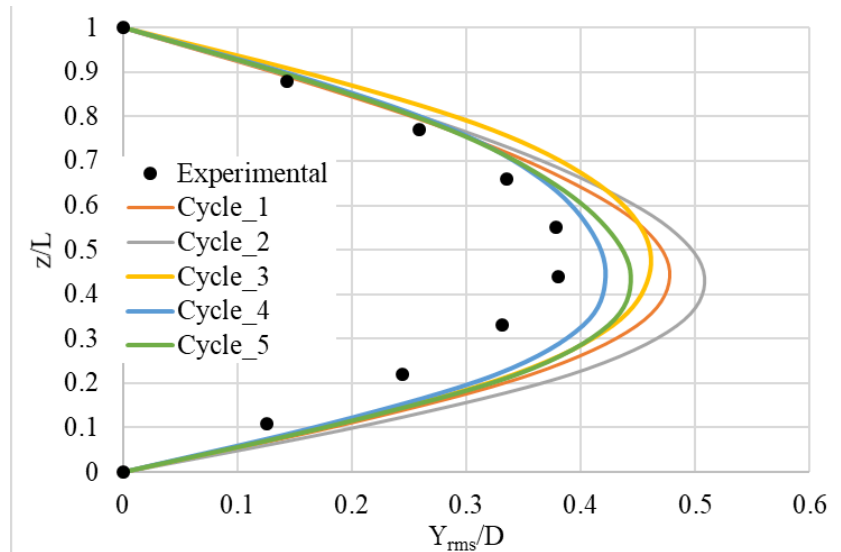


Figure 4.30. Comparison of data from difference oscillation cycles in cross-flow (CF) direction on the coarse mesh

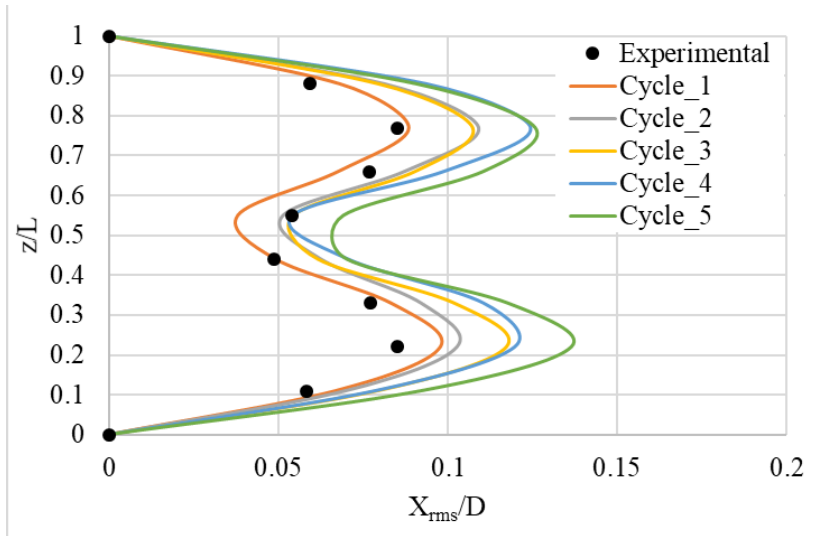


Figure 4.31. Comparison of data from difference oscillation cycles in in-line (IL) direction on the fine mesh

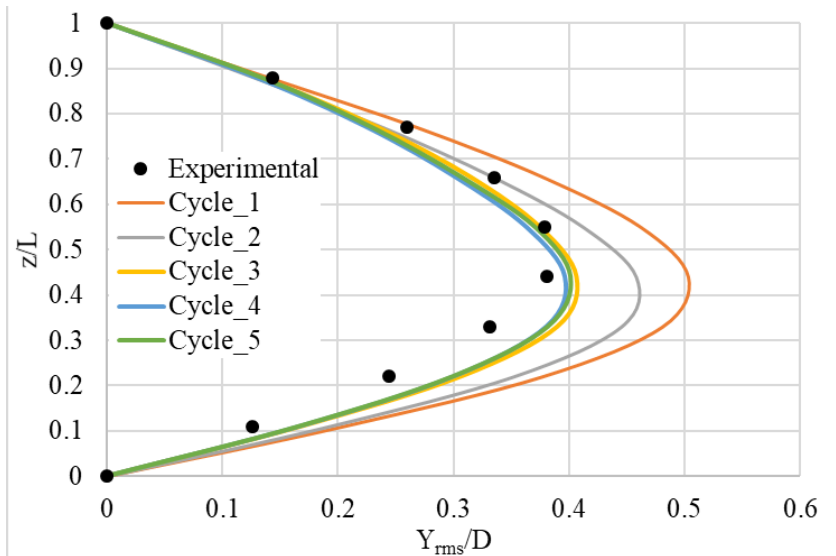


Figure 4.32. Comparison of data from difference oscillation cycles in cross-flow (CF) direction on the fine mesh

4.6 The Riser Dynamic Response

Figure 4.33 and Figure 4.34 illustrate the comparison of the envelopes of the IL and CF displacements from the simulations using the fine mesh and the coarse mesh with the experimental data for a freestream velocity of 0.2 m/s.

The IL response frequency may be estimated to be approximately twice the CF response frequency. This means the IL mode number is double the CF mode number for a tensioned string. It can be seen from the plots that the simulated data is in good agreement with the experimental data. From these plots, it can be noted that the IL vibration is the second mode while CF vibration is the first mode.

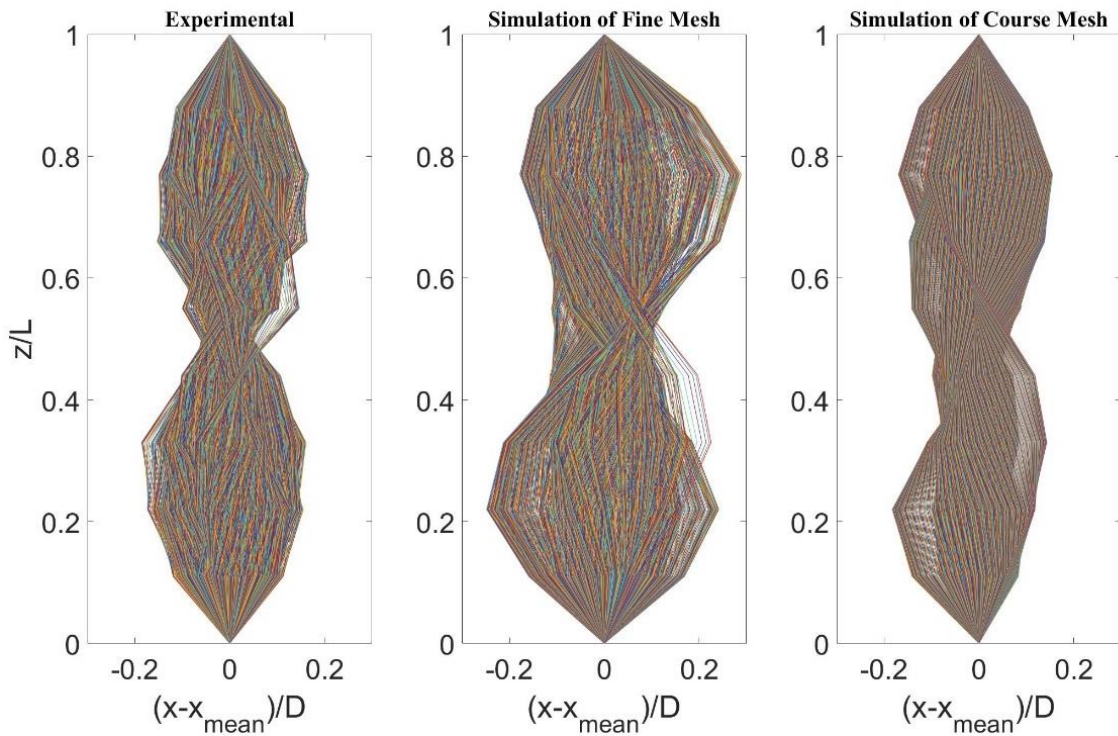


Figure 4.33. Comparison of the envelopes in IL direction at a velocity of 0.2 m/s

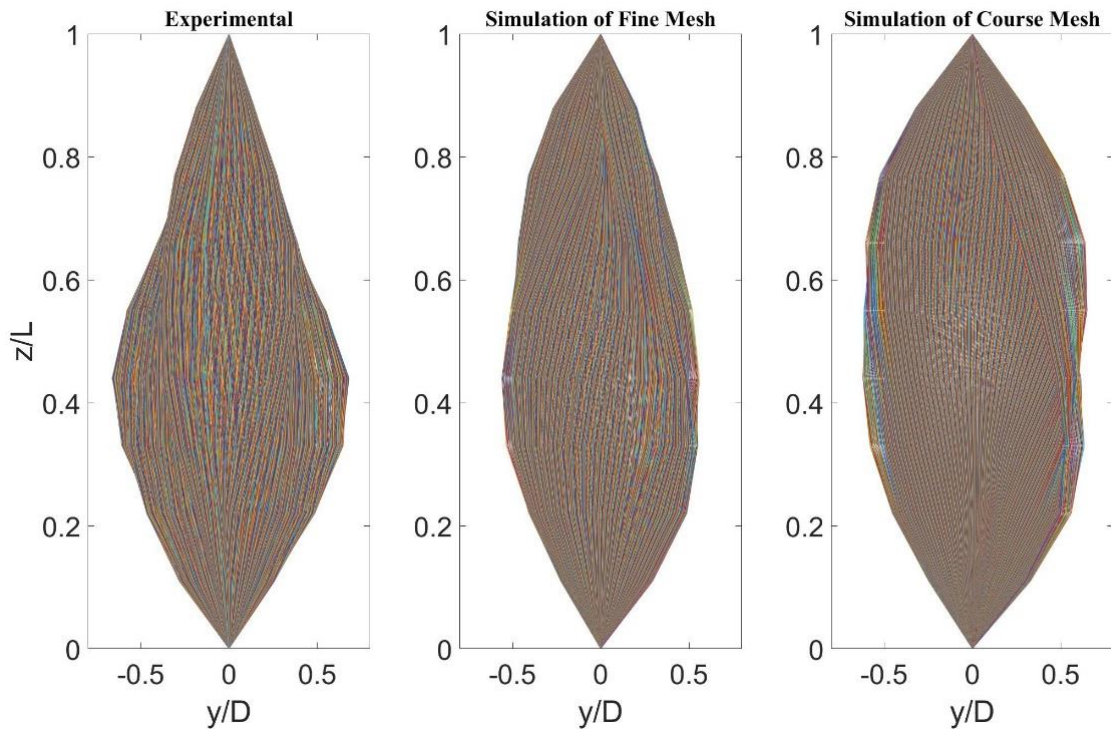


Figure 4.34. Comparison of the envelopes in CF direction at a velocity of 0.2 m/s

4.7 Comparison of RMS values of the Amplitudes of Oscillation with Experimental Data for a Freestream Velocity of 0.42 m/s

FSI analysis of the flexible riser in a uniform current velocity of 0.42 m/s using the coarse and fine meshes. The different parameters that are used in this analysis are same as the ones that are used for the freestream velocity of 0.2 m/s. The computed RMS values of the amplitude of vibrations in IL and CF directions are compared with the experimental data by Lehn (Lehn, 2003). Figure 4.33 shows the comparison of the RMS amplitudes in IL direction on the coarse and the fine meshes and Figure 4.34 shows the RMS values of the amplitude of vibrations in the CF direction. It can be seen from these figures that the results from the simulation using the coarse mesh matches well with the

experimental data, while the results from the fine mesh show deviation from the experimental data. Further analysis is needed to resolve this issue.

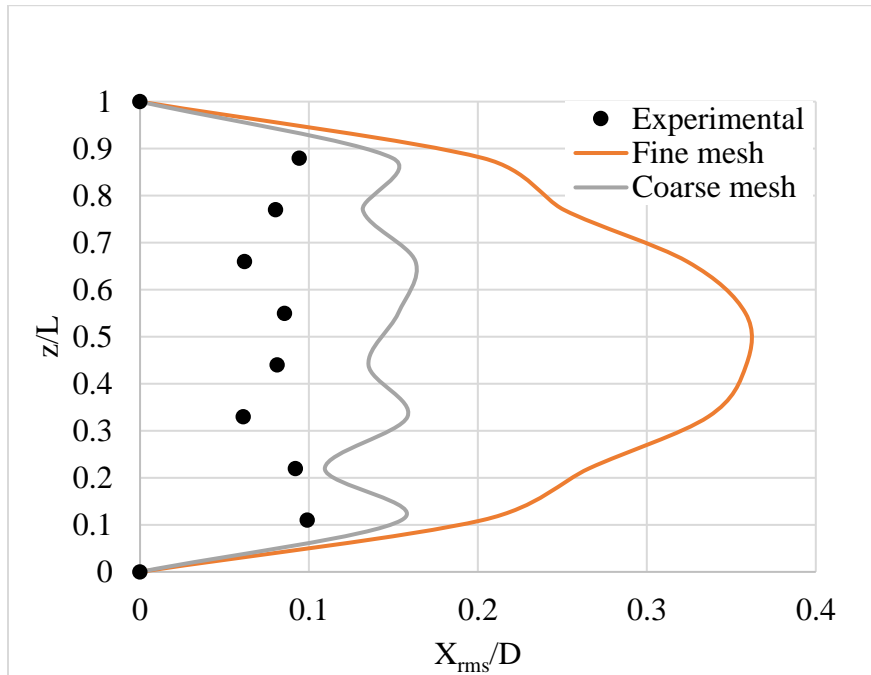


Figure 4.35. Comparison of the RMS amplitudes in IL direction on the fine mesh with published data at velocity = 0.42 m/s

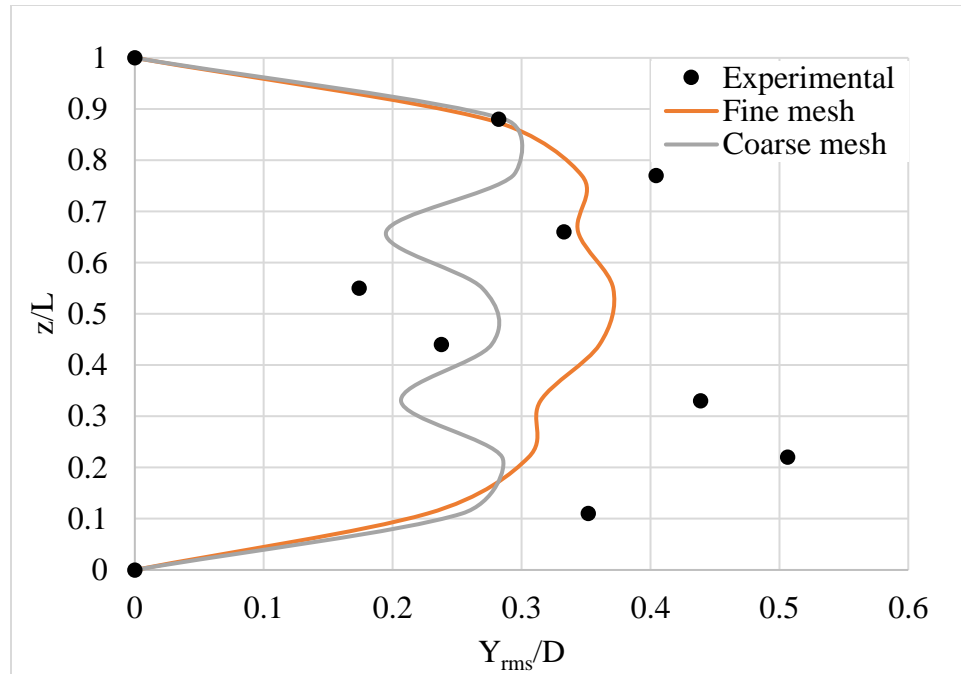


Figure 4.36. Comparison of the RMS amplitudes in CF direction on the fine mesh with published data at velocity = 0.42 m/s

CHAPTER 5 SUMMARY

Vortex shedding is an oscillating flow behind blunt bodies when fluid flows past it, which causes the vortex-induced vibrations (VIV). A few of the examples of engineering systems in which VIV is predominant include bridges, heat exchangers, marine cables, electrical power lines, and petroleum risers. A critical application of VIV is the risers used in petroleum industries, which connects between sea surface and sea base. A failure of risers and platforms can result in enormous economic and catastrophic environmental problems. Therefore, understanding VIV is essential to estimate fatigue damage of the offshore systems and this thesis describes a numerical method to analyze VIV using a fluid-structure interaction (FSI) approach.

Analysis of VIV of a flexible riser in the uniform current is simulated using different components that are available in ANSYS software. Each of the components needed to conduct an FSI analysis is validated using benchmark results. These components include modal analysis to determine the mode shapes and frequencies, fluid flow analysis to determine the vortex shedding frequency, and the coupled simulation to determine the structural response under the action of fluid forces. The results from the modal analysis are compared with the theoretical results from the tensed string and non-stressed beam, and they are found to be in good agreement with each other. The Strouhal number corresponding to the vortex shedding from the rigid riser is compared with the experimental results for a circular cylinder.

FSI analysis of flexible riser is validated using the experimental data from the MARINTEK by ExxonMobil Upstream Research Company (URC). The computed RMS values of the amplitude of vibrations in the in-line (IL) and cross-flow (CF) directions are compared with the experimental data. FSI analysis is carried out using two different freestream velocities, $V= 0.2$ m/s and $V= 0.42$ m/s, with two different meshes. The results from the computations using a uniform velocity of 0.2 m/s, for the two different meshes, are in good agreement with the model test result for ExxonMobil. For freestream velocity of 0.2 m/s, the IL and CF vibrations are dominated by the second mode and the first mode, respectively. As expected, based on the excitation of dominant modes, the effect of VIV in the IL direction is more predominant than in the CF direction. The computed results using the coarse mesh for the uniform velocity of 0.42 m/s is not in good agreement with the experimental data. However, the simulated results deviate from the experimental data for the fine mesh. Further study is needed to resolve this issue.

In summary, a numerical approach is presented to analyze the VIV response of a flexible riser under uniform velocities. The computed results showed agreement with the experimental results and riser subject to the uniform velocity, which demonstrates that this method is dependable and capable of predicting VIV response. Therefore, this validated model could be used for the estimation of the effectiveness of VIV suppression systems for flexible risers, as an alternative to experimental testing.

CHAPTER 6 FUTURE WORK

Preliminary work has been conducted to evaluate dynamic behavior of VIV suppression system for risers. The details of the geometry of the suppression system, data from the modal analysis, and fluid flow analysis are presented in the following sections. However, a coupled fluid-structure interaction analysis is needed to complete this study.

6.1 The Geometry of the Riser with Fairings

A sketch of the suggested fairing is shown in Figure 6.1. The length of the fairing is 78 mm and the radius of the frontal area is 18mm. The fairing is assumed to be made from plastic. The properties of the material were chosen from the Engineering Database in ANSYS for polyethylene. Base on this database, the density, Young's Modulus and Poisson's ratio are set as 7850 kg/m^3 , $2\text{E}+11 \text{ Pa}$ and 0.3, respectively.

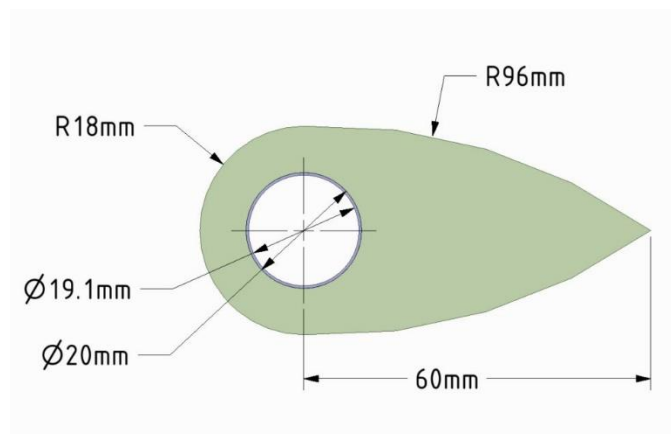


Figure 6.1. The top view of the riser with the fairing

6.2 The Geometry of the Riser with the Strakes

The second VIV suppression system considered for the analysis is a triple helical strake made from a silicone with the specified pitch-to-diameter ratio of 16 material and glued to the riser model. The strakes had a triangular shape with a height of 5 mm and a length of 6.38 mm. The top view of this strakes is shown in Figure 6.2. The density, Young's Modulus, and Poisson's ratio for silicone are set as 2330 kg/m³, 1.25E+11 Pa and 0.27, respectively.

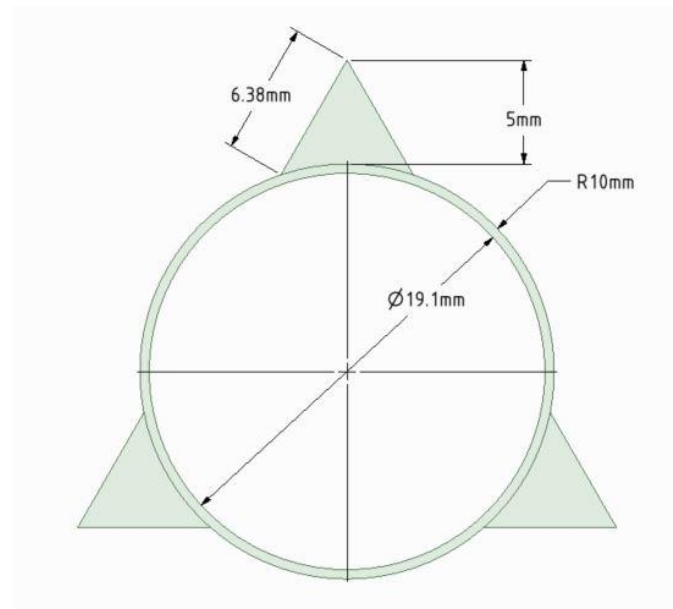


Figure 6.2. The top view of the riser with the strakes

6.3 Modal Analysis for Riser with Suppression

Using the same approach that is described in Chapter 4, the Eigen frequencies of the first eight modes for risers with fairings and strakes are estimated using modal analysis in ANSYS. In this simulation, the riser with the suppression systems are assumed to be pre-stressed with 817N. The results from these computations for the

flexible riser with the fairing and the strakes are tabulated in Table 10 and Table 11, respectively.

Mode	Direction	FEA (Hz)
1	IL	0.99122
	CF	1.0558
2	IL	2.0926
	CF	2.4701
3	IL	3.3965
	CF	4.523
4	IL	4.9703
	CF	6.8587
5	IL	7.2231
	CF	9.0933
6	IL	10.703
	CF	11.694
7	IL	14.686
	CF	14.879
8	IL	18.079
	CF	19.857

Table 10. Eigenfrequencies for the flexible riser with the fairing

Mode	Direction	FEA (Hz)
1	IL	1.8121
	CF	1.8125
2	IL	3.8193
	CF	3.8199
3	IL	6.1862
	CF	6.1876
4	IL	9.0288
	CF	9.0297
5	IL	12.436
	CF	12.437
6	IL	16.445
	CF	16.447
7	IL	21.086
	CF	21.088
8	IL	26.389
	CF	26.392

Table 11. Eigenfrequencies for the flexible riser with the strakes

6.4 Fluid Analysis of the Riser with the Fairing

Similar to the bare riser discussed in Chapter 4, the computational domain for the fluid analysis for riser with fairing is discretized using a multi-block approach. Figure 6.3 shows the top view of the block structure used for the discretization of the computational domain. Using the edge sizing option in Mesher, the number of divisions for the segments A, B, C, D, E, F, and G are set as 32, 40, 32, 80, 80, 20, and 64, respectively, as shown in Figure 6.4. The number of divisions along the axial direction is set as 20. The mesh in the top plane and a zoomed view of the mesh around the fairing are shown in Figure 6.5 and Figure 6.6, respectively. A 3-dimensional mesh is generated by extruding the mesh on the top plane along the axial direction. This resulted in a mesh with 502720 elements as shown in Figure 6.7.

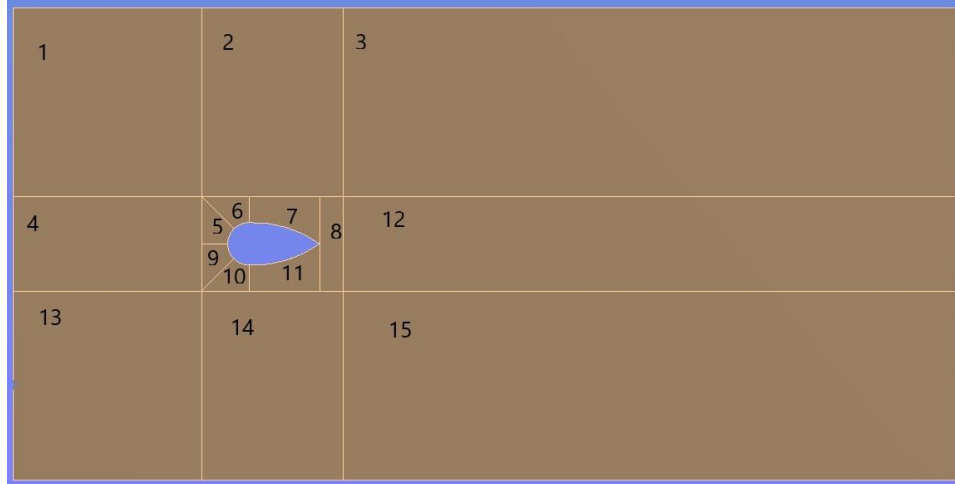


Figure 6.3. Block structure on top XY-plane

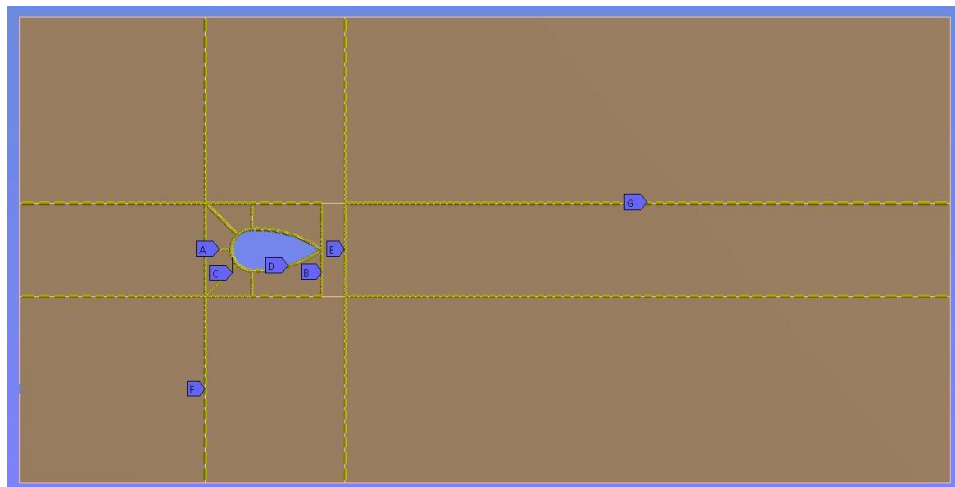


Figure 6.4. The number of divisions on the selected boundary segments

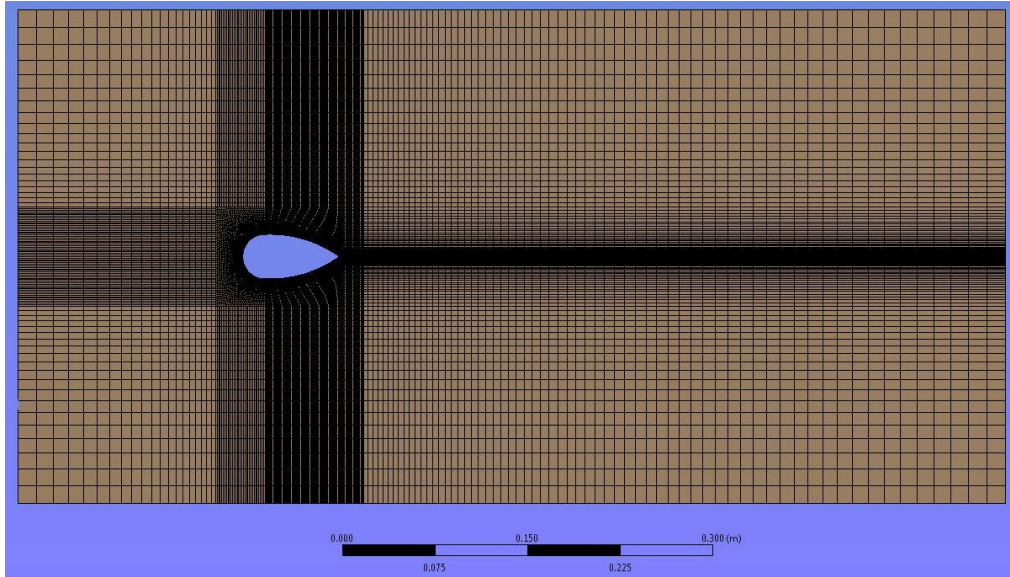


Figure 6.5. Mesh on top XY-plane

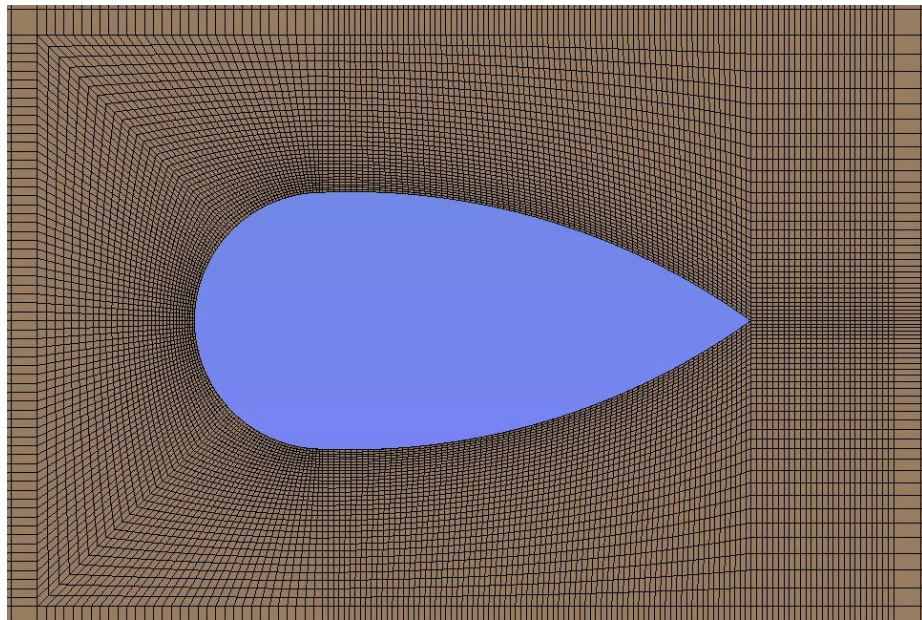


Figure 6.6. Mesh around the fairing

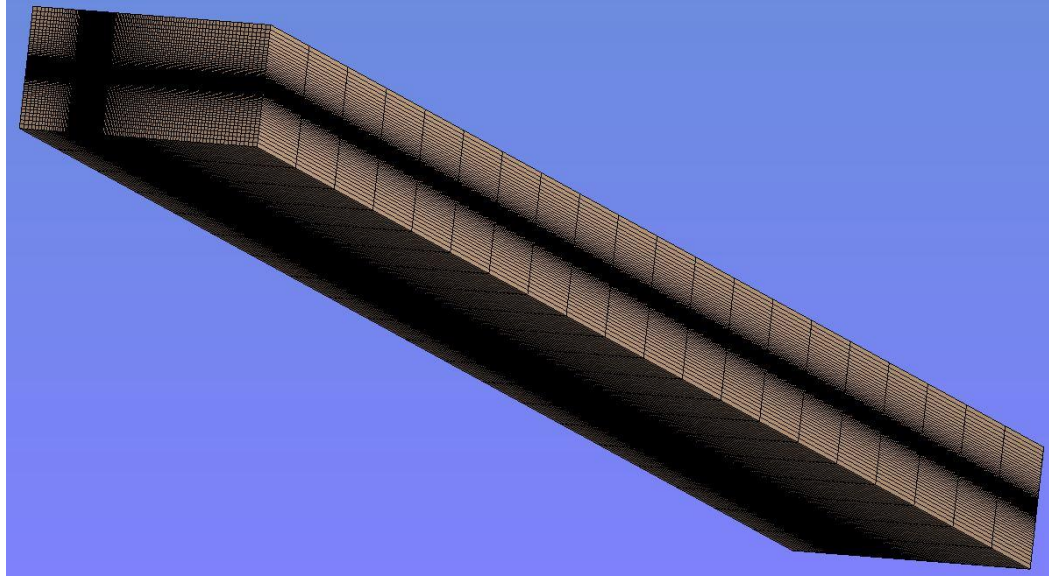


Figure 6.7. Overall view of the coarse mesh

The incompressible form of the Navier-Stokes equation, given in Chapter 3, is taken as the governing equation for the fluid flow and the eddy viscosity is estimated using the SST κ - ω turbulence model. For the unsteady simulations, the time step size is set as 0.001 s, and the number of iterations as 10000. To resolve the unsteady flow accurately, a maximum of 20 sub-iterations are used in each time. Flow simulations are carried out for uniform velocities of 0.2 m/s. A Fourier analysis of the time history of lift coefficient is used to calculate the vortex shedding frequency and the Strouhal number. The power-spectral frequency of the lift coefficient for the freestream velocity of 0.2 m/s is shown in Figure 6.8.

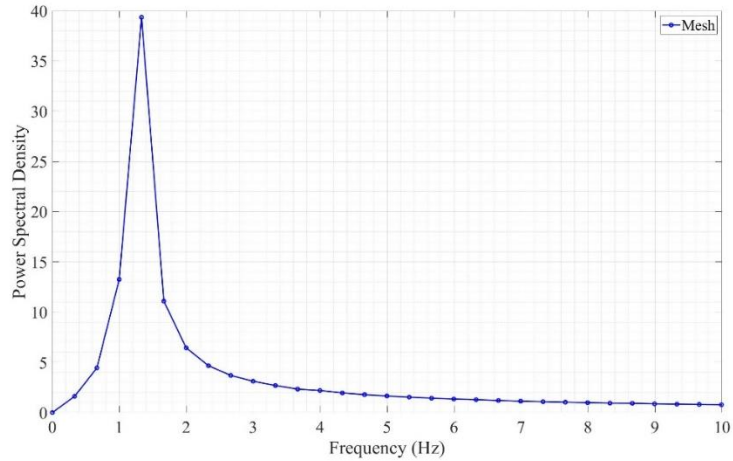


Figure 6.8. Power spectral density from lift history for the flow with a freestream velocity of 0.2 m/s

The vortex shedding frequencies and the corresponding Strouhal numbers are summarized in Table 12. The predicted Strouhal number for the riser with fairing is 0.239, which is comparable to the Strouhal number of 0.22 for the bare riser. The predicted velocity distribution from the simulation at axial distances of $z/L= 0, 0.25, 0.5, 0.75,$ and 1 is shown in Figure 6.9. Vortex shedding from the riser is evident in this figure. Further analysis is required to estimate the dynamic behavior of the riser with fairings.

Diameter [m]	0.02			
Velocity [m/s]	Reynolds Number	According to	Frequency	Strouhal Number
0.2	7165.543	Lift Coefficient	1.332	0.239

Table 12. Frequency and Strouhal number from fluid flow analysis

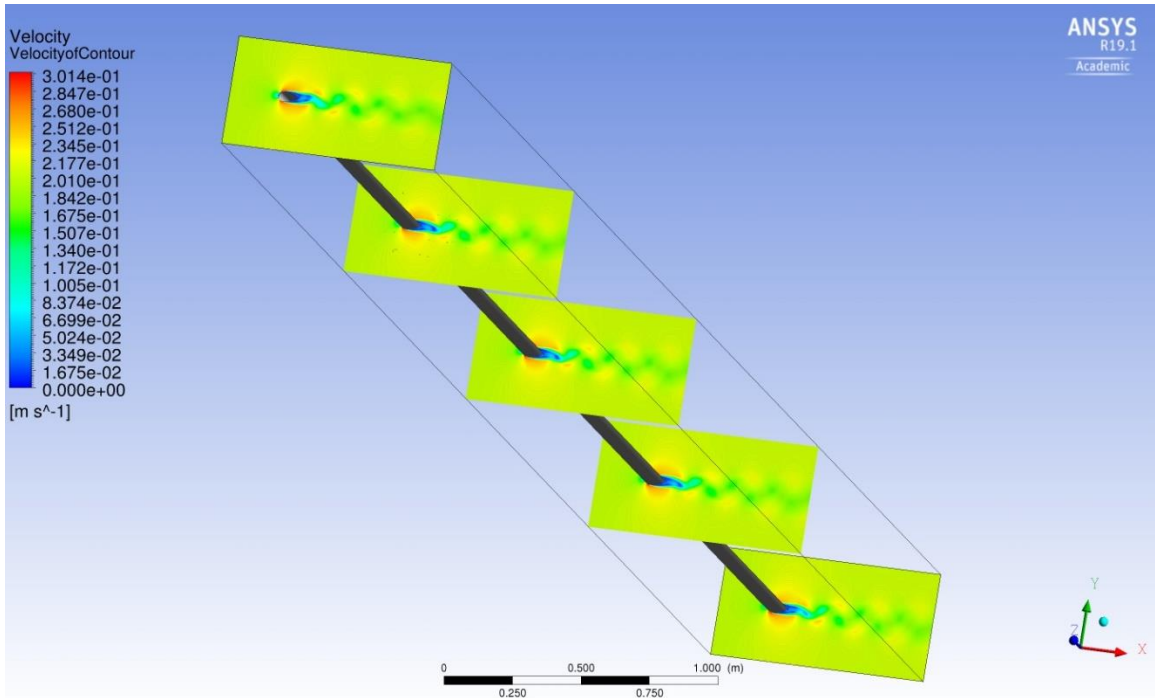


Figure 6.9. Vortex shedding at $z/L = 0, 0.25, 0.5, 0.75, 1$ of the riser with the fairing at freestream velocity, 0.2 m/s

REFERENCES

- Bearman, P. W., & Owen, J. C. (1998). REDUCTION OF BLUFF-BODY DRAG AND SUPPRESSION OF VORTEX SHEDDING BY THE INTRODUCTION OF WAVY SEPARATION LINES. *Journal of Fluids and Structures*, 12(1), 123-130. doi:<https://doi.org/10.1006/jfls.1997.0128>
- Blevins, R. D. (1990). *Flow-induced vibration*.
- Blevins, R. D., & Plunkett, R. (1980). Formulas for natural frequency and mode shape. In: American Society of Mechanical Engineers.
- Cengel, Y. A. (2010). *Fluid mechanics*: Tata McGraw-Hill Education.
- Choi, H., Jeon, W.-P., & Kim, J. (2008). Control of Flow Over a Bluff Body. *Annual Review of Fluid Mechanics*, 40(1), 113-139. doi:10.1146/annurev.fluid.39.050905.110149
- Chung, J., & Hulbert, G. (1993). A time integration algorithm for structural dynamics with improved numerical dissipation: the generalized- α method. *Journal of applied mechanics*, 60(2), 371-375.
- Every, M. J., King, R., & Weaver, D. S. (1982). Vortex-excited vibrations of cylinders and cables and their suppression. *Ocean Engineering*, 9(2), 135-157. doi:[https://doi.org/10.1016/0029-8018\(82\)90010-5](https://doi.org/10.1016/0029-8018(82)90010-5)
- Frank, W. R., Tognarelli, M. A., Slocum, S. T., Campbell, R. B., & Balasubramanian, S. (2004, 2004). *Flow-induced vibration of a long, flexible, straked cylinder in uniform and linearly sheared currents*.
- Gao, Y., Fu, S., Ren, T., Xiong, Y., & Song, L. (2015). VIV response of a long flexible riser fitted with strakes in uniform and linearly sheared currents. *Applied Ocean Research*, 52(Supplement C), 102-114. doi:10.1016/j.apor.2015.05.006
- Gao, Y., Yang, J., Xiong, Y., Wang, M., & Peng, G. (2016). Experimental investigation of the effects of the coverage of helical strakes on the vortex-induced vibration response of a flexible riser. *Applied Ocean Research*, 59(Supplement C), 53-64. doi:10.1016/j.apor.2016.03.016
- Huang, K., Chen, H.-C., & Chen, C.-R. (2010). Vertical riser VIV simulation in uniform current. *Journal of Offshore Mechanics and Arctic Engineering*, 132(3), 031101.

- Huang, K., Chen, H.-C., & Chen, C.-R. (2011). Numerical scheme for riser motion calculation during 3-D VIV simulation. *Journal of Fluids and Structures*, 27(7), 947-961. doi:10.1016/j.jfluidstructs.2011.06.010
- Jahanmiri, M. (2010). *Active flow control: a review*. Retrieved from
- Jaiswal, V., & Vandiver, J. K. (2007). *VIV response prediction for long risers with variable damping*. Paper presented at the ASME 2007 26th International Conference on Offshore Mechanics and Arctic Engineering.
- Kármán, T. v. (1994). *Aerodynamics*.
- Khorasanchi, M., & Huang, S. (2014). Instability analysis of deepwater riser with fairings. *Ocean Engineering*, 79, 26-34. doi:<https://doi.org/10.1016/j.oceaneng.2014.01.003>
- Kral, L. D. (2000). Active flow control technology. *ASME FED, Technical Brief*, 1-28.
- Lehn, E. (2003). VIV suppression tests on high L/D flexible cylinders (main report). *ExxonMobil upstream research company*.
- Ley, J., & el Moctar, O. (2014). *An Enhanced 1-Way Coupling Method to Predict Elastic Global Hull Girder Loads*. Paper presented at the ASME 2014 33rd International Conference on Ocean, Offshore and Arctic Engineering.
- Liao, J.-C. (2001). *Vortex-induced vibration of slender structures in unsteady flow*. Massachusetts Institute of Technology,
- Mukundan, H., Modarres-Sadeghi, Y., Dahl, J. M., Hover, F. S., & Triantafyllou, M. S. (2009). Monitoring VIV fatigue damage on marine risers. *Journal of Fluids and Structures*, 25(4), 617-628. doi:<https://doi.org/10.1016/j.jfluidstructs.2009.03.003>
- Newman, D. J., & Karniadakis, G. E. (1997). A direct numerical simulation study of flow past a freely vibrating cable. *Journal of Fluid Mechanics*, 344, 95-136.
- Sarpkaya, T. (2004). A critical review of the intrinsic nature of vortex-induced vibrations. *Journal of Fluids and Structures*, 19(4), 389-447. doi:<https://doi.org/10.1016/j.jfluidstructs.2004.02.005>
- Taylor, G. K., Nudds, R. L., & Thomas, A. L. (2003). Flying and swimming animals cruise at a Strouhal number tuned for high power efficiency. *Nature*, 425(6959), 707.
- Timoshenko, S., Young, D., & Weaver, J. W., 1974. *Vibration Problems in Engineering*. ed: John Wiley and Sons, New York.

- Trim, A. D., Braaten, H., Lie, H., & Tognarelli, M. A. (2005). Experimental investigation of vortex-induced vibration of long marine risers. *Journal of Fluids and Structures*, 21(3), 335-361. doi:<https://doi.org/10.1016/j.jfluidstructs.2005.07.014>
- Vandiver, J. K., Swithenbank, S., Jaiswal, V., & Marcollo, H. (2006). *The Effectiveness of Helical Strakes in the Suppression of High-Mode-Number VIV*. Paper presented at the Offshore Technology Conference, Houston, Texas, USA.
- Wilcox, D. C. (1998). *Turbulence modeling for CFD* (Vol. 2): DCW industries La Canada, CA.
- Zdravkovich, M. M. (1981). Review and classification of various aerodynamic and hydrodynamic means for suppressing vortex shedding. *Journal of Wind Engineering and Industrial Aerodynamics*, 7(2), 145-189. doi:[https://doi.org/10.1016/0167-6105\(81\)90036-2](https://doi.org/10.1016/0167-6105(81)90036-2)